

MORPHOTECTONIC ANALYSIS AND KINEMATIC EVOLUTION OF THE  
CENTRAL GEDİZ ALAŞEHİR GRABEN, WESTERN ANATOLIA, TURKEY

A THESIS SUBMITTED TO  
THE GRADUATE SCHOOL OF NATURAL AND APPLIED SCIENCES  
OF  
MIDDLE EAST TECHNICAL UNIVERSITY

BY

TAMER DÖNMEZOĞULLARI

IN PARTIAL FULFILLMENT OF THE REQUIREMENTS  
FOR  
THE DEGREE OF MASTER OF SCIENCE  
IN  
GEOLOGICAL ENGINEERING

AUGUST 2019



Approval of the thesis:

**MORPHOTECTONIC ANALYSIS AND KINEMATIC EVOLUTION OF  
THE CENTRAL GEDİZ ALAŞEHİR GRABEN, WESTERN ANATOLIA,  
TURKEY**

submitted by **TAMER DÖNMEZOĞULLARI** in partial fulfillment of the requirements for the degree of **Master of Science in Geological Engineering Department, Middle East Technical University** by,

Prof. Dr. Halil Kalıpçılar  
Dean, Graduate School of **Natural and Applied Sciences**

\_\_\_\_\_

Prof. Dr. Erdin Bozkurt  
Head of Department, **Geological Engineering**

\_\_\_\_\_

Prof. Dr. Bora Rojay  
Supervisor, **Geological Engineering, METU**

\_\_\_\_\_

**Examining Committee Members:**

Prof. Dr. Erdin Bozkurt  
Geological Engineering, METU

\_\_\_\_\_

Prof. Dr. Bora Rojay  
Geological Engineering, METU

\_\_\_\_\_

Prof. Dr. Mehmet Lütfi Süzen  
Geological Engineering, METU

\_\_\_\_\_

Assist. Prof. Dr. Fatma Toksoy Köksal  
Geological Engineering, METU

\_\_\_\_\_

Prof. Dr. Veysel Işık  
Geological Engineering, Ankara University

\_\_\_\_\_

Date: 28.08.2019

**I hereby declare that all information in this document has been obtained and presented in accordance with academic rules and ethical conduct. I also declare that, as required by these rules and conduct, I have fully cited and referenced all material and results that are not original to this work.**

Name, Surname: Tamer Dönmezoğulları

Signature:

## ABSTRACT

### **MORPHOTECTONIC ANALYSIS AND KINEMATIC EVOLUTION OF THE CENTRAL GEDİZ ALAŞEHİR GRABEN, WESTERN ANATOLIA, TURKEY**

Dönmezoğulları, Tamer  
Master of Science, Geological Engineering  
Supervisor: Prof. Dr. Bora Rojay

August 2019, 81 pages

The Gediz Alaşehir Graben (GAG) is one of the seismically active grabens within western Anatolia. The study area is located at the center of this graben. It is aimed to evaluate the post-Miocene tectonic evolution of the GAG in terms of structural and morphometric analyses. The dominant trends of the Pliocene and Miocene sequences are mainly in NW-SE direction and are almost parallel to each other. Three fault clusters were determined for the region from a length weighted rose diagram, and the general trend is mainly in NW-SE direction. 120 slip-data were used to analyze the region in terms of kinematic evolution. The relationship between  $\sigma_1$  and  $\sigma_3$  was used as the main evaluating tools for the kinematic analysis. The results of the analysis show dominantly NNE-SSW pure extension, and according to  $\sigma_1$  which is the vertical principal axis, the fault type was defined as a normal fault. In this context, under the control of these normal fault activities, horst-graben structures were defined within the study area. The asymmetry and the fault activity of the region were studied in terms of morphometry. To define the asymmetry along the ridges, the slope changes and the asymmetry ratio were applied, and the results indicate the ridges are asymmetric depending on the faulting along the northeast sides of the ridges. The Smf index was applied along Manisa Fault, Gölarmara Fault and northeast of Çaldağ.

According to the Smf results, the activity of the region in terms of active faulting was defined, and the results and reasons for this index were evaluated by considering lithology. In conclusion, all results were discussed in this study in details in terms of kinematic evolution and morphometric analysis.

Keywords: Western Anatolia, Gediz Alaşehir Graben, kinematic evolution, asymmetry, mountain front sinuosity

## ÖZ

### **GEDİZ ALAŞEHİR GRABENİ MERKEZİNİN MORFOTEKTONİK ANALİZİ VE KİNEMATİK EVRİMİ, BATI ANADOLU, TÜRKİYE**

Dönmezoğulları, Tamer  
Yüksek Lisans, Jeoloji Mühendisliği  
Tez Danışmanı: Prof. Dr. Bora Rojay

Ağustos 2019, 81 sayfa

Gediz Alaşehir Graben'i (GAG), Batı Anadolu'daki sismik açıdan aktif grabenlerden biridir. Çalışma alanı bu grabenin merkezinde bulunmaktadır. GAG'nin Miyosen sonrası tektonik evriminin yapısal ve morfometrik analizler açısından değerlendirilmesi amaçlanmaktadır. Pliyosen ve Miyosen dizilerinin baskın eğilimleri temel olarak NW-SE yönündedir ve neredeyse birbirine paraleldir. Bölge için uzunluk ağırlıklı bir gül diyagramından üç fay kümesi belirlenmiştir ve genel eğilim çoğunlukla NW-SE yönündedir. Bölgeyi kinematik evrim açısından analiz etmek için 120 kayma-verisi kullanılmıştır.  $\sigma_1$  ve  $\sigma_3$  arasındaki ilişki, kinematik analiz için ana değerlendirme araçları olarak kullanıldı. Analiz sonuçları baskın olarak NNE-SSW saf gerilmesini göstermektedir ve dikey ana eksen olan  $\sigma_1$ 'e göre, fay tipi normal fay olarak tanımlanmıştır. Bu bağlamda, çalışma alanı içerisinde bu normal fay aktivitelerinin kontrolü altında horst-graben yapıları tanımlanmıştır. Bölgenin asimetrisi ve fay aktivitesi morfometri yönünden incelenmiştir. Sırtlar boyunca asimetriyi tanımlamak için, eğim değişimleri ve asimetri oranı uygulanmıştır ve sonuçlar sırtların kuzeydoğu kenarlarındaki faylara bağlı olarak asimetric olduğunu gösterir. Smf indeksi Manisa Fayı, Gölarmara Fayı ve Çaldağ'ın kuzeydoğusunda uygulandı. Smf sonuçlarına göre, bölgenin aktif faylanma açısından etkinliği tanımlanmış ve bu endeksin sonuçları ve nedenleri litoloji dikkate alınarak

değerlendirilmiştir. Sonuç olarak, bu çalışmada tüm sonuçlar kinematik evrim ve morfometrik analizler açısından detaylı bir şekilde tartışılmıştır.

Anahtar Kelimeler: Batı Anadolu, Gediz Alaşehir Grabeni, kinematik evrim, asimetri, dağ önü kıvrımlılığı

To my father Yaşar Dönmezoğulları...

## ACKNOWLEDGEMENTS

First of all, I would like to express my deepest gratitude to my supervisor Prof. Dr. Bora Rojay for his guidance, support, motivation and trust in me.

I would like to thank my thesis committee, Prof. Dr. Erdin Bozkurt, Prof. Dr. Mehmet Lütü Süzen, Assist. Prof. Dr. Fatma Toksoy Köksal and Prof. Dr. Veysel Işık for their valuable advice and comments about my thesis.

I would like to express my sincere gratitude to my family, my father Yaşar Dönmezoğulları, my mother Sezer Dönmezoğulları and my brothers Alper Dönmezoğulları and Dinçer Dönmezoğulları for their endless love and patience.

My special thanks to Ümran Yiğit, who never give up listening to me. She was always with me with her endless support, encouragement and patience. This process could not have been completed without her.

My final thanks to my father Yaşar Dönmezoğulları, who always supports me, tries to solve my problem instantly, always guides and encourages me. I will never forget you...

## TABLE OF CONTENTS

ABSTRACT .....	v
ÖZ .....	vii
ACKNOWLEDGEMENTS .....	x
TABLE OF CONTENTS .....	xi
LIST OF TABLES .....	xiii
LIST OF FIGURES .....	xiv
CHAPTERS	
1. INTRODUCTION .....	1
1.1. Purpose and Scope.....	1
1.2. Geographic Location .....	3
1.3. Method of Study .....	3
1.4. Previous Studies .....	5
1.4.1. Regional Tectonic Settings .....	5
1.4.2. The Gediz Alaşehir Graben (GAG).....	8
1.4.3. Morphometric Studies .....	12
2. STRATIGRAPHY .....	15
3. STRUCTURAL GEOLOGY .....	19
3.1. Attitude of the Bedding Planes.....	19
3.2. Attitude of the Faults .....	21
3.3. Kinematic Analysis of the Faults .....	22
3.3.1. Çınaroba (Northwest of Çaldağ Ridge) .....	24
3.3.2. Halitpaşa (Northwest of Çaldağ Ridge).....	25

3.3.3. Değnekler (Değnekler Ridge) .....	27
3.3.4. Lütfiye (Northwest of Değnekler Ridge) .....	28
3.3.5. Gölarmara (Gölarmara Ridge) .....	30
3.3.6. Sancaklıkayadibi (Spil Mountain).....	31
3.3.7. The Manisa Fault.....	35
3.3.8. The Akhisar Fault (Karahöyük Mountain).....	43
4. MORPHOMETRIC ANALYSIS .....	49
4.1. Asymmetry along the Ridges.....	49
4.1.1. The Çaldağ Ridge.....	54
4.1.2. The Değnekler Ridge.....	57
4.1.3. The Gölarmara Ridge .....	60
4.2. The Mountain Front Sinuosity (Smf).....	63
5. DISCUSSION .....	67
6. CONCLUSION .....	73
6.1. Results of Structural Geology .....	73
6.2. Results of Morphometric Analysis .....	74
REFERENCES .....	77

## LIST OF TABLES

### TABLES

Table 3.1. The principal stress axes and the R-value results for the Manisa Fault at Location 01. ....	36
Table 3.2. The principal stress axes and the ratio of principal stress differences results for the North Akhisar Fault. ....	45
Table 3.3. The principal stress axes and the ratio of principal stress differences results for the South Akhisar Fault. ....	47
Table 4.1. The range of slope change with color legend for slope modeling. ....	52
Table 4.2. Lithological units with defined letters for cross sections. ....	53
Table 4.3. Asymmetry ratio results determined for each ridge. ....	63

## LIST OF FIGURES

### FIGURES

Figure 1.1. Regional geological map showing the location map of Gediz Graben (BM: Büyük Menderes graben, KM: Küçük Menderes graben, Gö: Gördes basin, De. Demirci basin, Se: Selendi basin, Gü. Güre basin, Da. Dağkızılca basin, Cu. Cumaovası basin, S. Selçuk basin, Ku. Kuşadası basin, Sö. Söke basin, A. Akköy basin, Bo. Bozdoğan basin, Ka. Karacasu basin (Bozkurt & Rojay, 2005). .....	2
Figure 1.2. Geographic setting of the study area. ....	3
Figure 1.3. Tectonic setting of eastern Mediterranean (Bozkurt & Rojay, 2005). .....	5
Figure 1.4. Geographic setting of the Gediz Alaşehir Graben. ....	9
Figure 2.1. Generalized geological map of the study area (partially compiled from Rojay and Toprak, 2001). ....	16
Figure 2.2. A-A' Cross Section along the study area. ....	17
Figure 2.3. Generalized tectono-stratigraphic columnar section of the study area; not to scale (Ages are from International Commission on Stratigraphy). ....	18
Figure 3.1. The rose diagram showing strike measurements taken from the bedding planes of the Pliocene sequences (n= 26). ....	20
Figure 3.2. The rose diagram showing strike measurements taken from the bedding planes of the Miocene sequence (n= 148). ....	20
Figure 3.3. The length weighted rose diagram of the faults showing the general trend within the study area. (The total number of recorded faults is 100 and total length is 189.3 cm in map scale). ....	21
Figure 3.4. Illustration showing the stress tensor types, stress symbols, stress ratio values and stress regime definitions (modified from Delvaux et al., 1997). ....	23
Figure 3.5. The principal stresses defining the fault type according to their orientation (Burg, 2017). ....	23

Figure 3.6. The fault plane studied in Çınaroba, Çaldağ has NW-SE trending with NE dipping (E: 559701, N: 4281354, Zone: 35). .....	24
Figure 3.7. The principal stress axes of the fault in Çınaroba, Çaldağ. ....	25
Figure 3.8. The fault plane studied in Halitpaşa, Çaldağ has NW-SE trending with NE dipping (E: 559705, N: 4281349, Zone: 35). .....	26
Figure 3.9. The principal stress axes of the fault in Halitpaşa, Çaldağ. ....	26
Figure 3.10. The fault plane studied in Değnekler has NW-SE trending with NE dipping (E: 572993, N: 4284830, Zone: 35). .....	27
Figure 3.11. The principal stress axes of the fault in Değnekler. ....	28
Figure 3.12. The fault plane studied in abandoned quarry located in the north of Lütfiye, Değnekler has NW-SE trending with NE dipping (E: 565072, N: 4288967, Zone: 35). .....	29
Figure 3.13. The principal stress axes of the fault in abandoned quarry located in the north of Lütfiye. ....	29
Figure 3.14. The fault plane studied in Gölarmara has NW-SE trending with NE dipping (E: 579504, N: 4284677, Zone: 35). .....	30
Figure 3.15. The principal stress axes of the fault in Gölarmara. ....	31
Figure 3.16. The first fault plane studied in Sancaklıkayadibi, Spil Mountain is 346°N-351°N trend with NE dipping (E: 545087, N: 4266406, Zone: 35). .....	32
Figure 3.17. The second fault plane obtained in Sancaklıkayadibi is 323°-326°N trend with NE dipping (E: 545136, N: 4266168, Zone: 35). ....	32
Figure 3.18. The principal stress axes of the all fault planes in Sancaklıkayadibi, Spil Mountain. ....	33
Figure 3.19. The faults studied in Sancaklıkayadibi, Spil Mountain have NE-SW extension. The fault located at north has 346°N-351°N trend and the fault located at south has 323°-326°N trend. ....	34
Figure 3.20. The locations where the slip-data have been collected and kinematic analysis has been studied along the Manisa Fault. ....	35
Figure 3.21. The fault plane showing three parts at Location 01 along the Manisa Fault (E: 544839, N: 4271464, Zone: 35). .....	36

Figure 3.22. The principal stress axes of all parts along the Manisa Fault.....	37
Figure 3.23. Sketch plan view of the fault plane observed at Location 01 along the Manisa Fault with stress symbols. ....	38
Figure 3.24. The fault plane evaluated at Location 02 has NW-SE trending with NE dipping (E: 545996, N: 4270827, Zone: 35).....	39
Figure 3.25. The principal stress axes of the fault plane examined at Location 02 along the Manisa Fault. ....	40
Figure 3.26. The fault plane evaluated at Location 03 has NW-SE trending with NE dipping (E: 546883, N: 4270145, Zone: 35).....	41
Figure 3.27. The principal stress axes of the fault plane examined at Location 03...	41
Figure 3.28. The kinematic map with stress symbols. A: Çınaroba Fault, B: Halitpaşa Fault, C: Değnekler Fault, D: Lütfiye Fault, E: Gölarmara Fault; F1 & F2: The faults evaluated in Sancaklıkayadibi, G1, G2 & G3: the Manisa Fault evaluated at three locations. ....	42
Figure 3.29. The location map of the Karahöyük Mountain Horst at south of Akhisar. ....	43
Figure 3.30. The map showing stress regime symbols of north and south Akhisar Fault with lithological units. ....	44
Figure 3.31. The principal stress axes of all parts along the North Akhisar Fault. ...	46
Figure 3.32. The principal stress axes of all parts along the South Akhisar Fault. ...	48
Figure 4.1. Slope map view showing degree changes in the region (Please see Figure 2.1 for the legend of generalized geological map). ....	50
Figure 4.2. Sketch draw showing surface slope in red colored arrows and stream channel slope in blue colored arrows.....	51
Figure 4.3. Water divide lines belonging to three ridges with streams obtained from ArcGIS 10.4.1 software. ....	52
Figure 4.4. The geology map showing profile lines for three ridges.....	53
Figure 4.5. 14 profiles drawn for the Çaldağ Ridge showing slope changes and the width of the profiles.....	55

Figure 4.6. 12 profiles drawn for the Değnekler Ridge showing slope changes and the width of the profiles. ....	58
Figure 4.7. 8 profiles drawn for the Gölarmara Ridge showing slope changes and the width of the profiles. ....	61
Figure 4.8. Determination of the asymmetry according to the width of the profile. .	62
Figure 4.9. Sketch draw showing how mountain front sinuosity (Smf) is calculated (modified from Keller & Pinter, 2002). ....	64
Figure 4.10. The map showing where the Smf index has been calculated with their results. The Smf value of the Manisa Fault is 1.21; the Smf value of the northeast margin of the Çaldağ is 1.50; the Smf value of the northeastern of the Gölarmara Ridge is 1.17. ....	65
Figure 5.1. The slope map model created for three mountain ridges according to determined slope changes in the profiles. ....	71
Figure 6.1. A tentative cross section along the study area. ....	75



## CHAPTER 1

### INTRODUCTION

#### 1.1. Purpose and Scope

Western Anatolia is known as one of the most important regions under the effect of tensional tectonics. This causes graben-horst systems that are nearly in E-W trending. There are many well developed grabens within Western Anatolia where the Gediz-Alaşehir Graben (GAG) is one of them (Figure 1.1). It is a part of Aegean Extensional Province (AEP). The length of the GAG were determined approximately 140-150 km and the width was defined as 15 km. In the western part, the width increases where the GAG merges with the Soma-Akhisar-Manisa basin.

The study area is a part of GAG and is located in the central part of the Gediz Alaşehir Graben where the width of the graben increases. There are many studies conducted in the region. Neotectonics, active tectonics and geology of the graben are still subject to many studies. Depending on the N-S extension of the Western Anatolia and escape Anatolia along Aegean Trench, generally E-W and NW-SE trending faults are observed, and the effects of these faults can be identified within the region clearly (Seyitoğlu & Scott, 1996b). Within the boundaries of the GAG the faults have different characteristics and minor structures.

The purpose of this thesis is to understand the post-Miocene tectonic evolution of the GAG by means of the analysis done on the strike/dip measurements of the bedding planes and fault slip-data and morphometric elements that are asymmetry of the ridges and the mountain front sinuosity. For this purpose, i) in order to conduct structural analysis, the strike/dip measurements of the bedding planes and faults, and slip-data from the fault planes observed within the study area were collected. Kinematic evolution of the region was studied according to slip-data of the fault planes ii)

morphologically the region was studied in terms of asymmetry and morphometry. According to the slope and width of profiles on the mountain ridges, asymmetry was analyzed. Asymmetry ratio based on width of mountain fronts was calculated for all three mountain ridges that are defined as Çaldağ Ridge, Değnekler Ridge, and Gölarmara Ridge. The mountain front sinuosity (Smf) index was applied to identify the tectonic activity of region, and the index was applied along the Manisa Fault, along the northeast margin of Çaldağ Ridge, and along the northeast margin of Gölarmara Ridge.

There are two basic criteria for the selection of the study area. These criteria are the fault activities occurring within the study area as a part of the GAG and the asymmetry formed due to this fault activities.

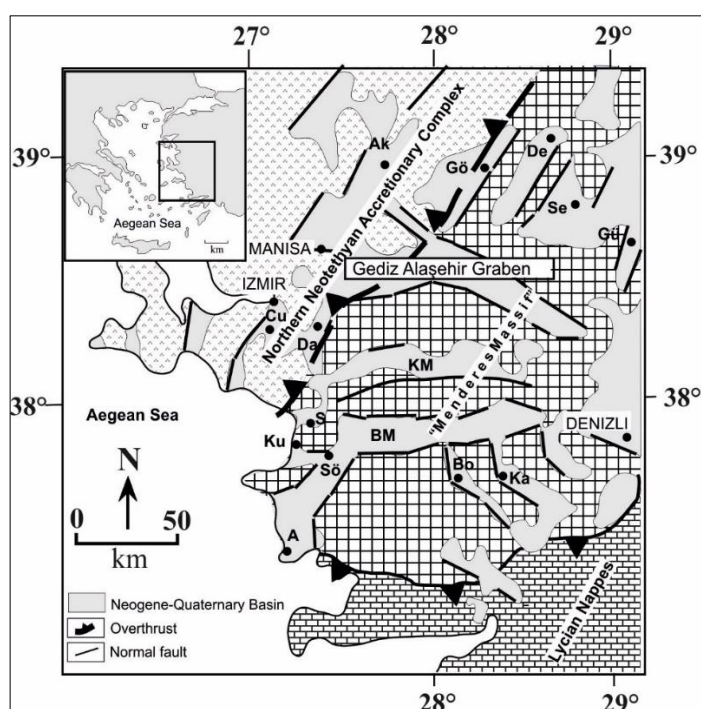


Figure 1.1. Regional geological map showing the location map of Gediz Graben (BM: Büyük Menderes graben, KM: Küçük Menderes graben, Gö: Gördes basin, De: Demirci basin, Se: Selendi basin, Gü: Güre basin, Da: Dağkızılca basin, Cu: Cumaovası basin, S: Selçuk basin, Ku: Kuşadası basin, Sö: Söke basin, A: Akköy basin, Bo: Bozdoğan basin, Ka: Karacasu basin (Bozkurt & Rojay, 2005).

## 1.2. Geographic Location

The study area is located at east of Manisa city center, at west of Marmara Lake, and at south of Beyoba which is the Manisa district. Moreover, at south, the study area is limited to Turgutlu and Ahmetli districts. The study area covers 16 topographic sheets having 1:25000 scale (Figure 1.2). These sheets are K19a3, K19a4, K19b3, K19b4, K19c1-c4, K19d1-d4, L19a1, L19a2, L19b1 and L19b2. It covers an area around 1445 km<sup>2</sup> (Figure 1.2).

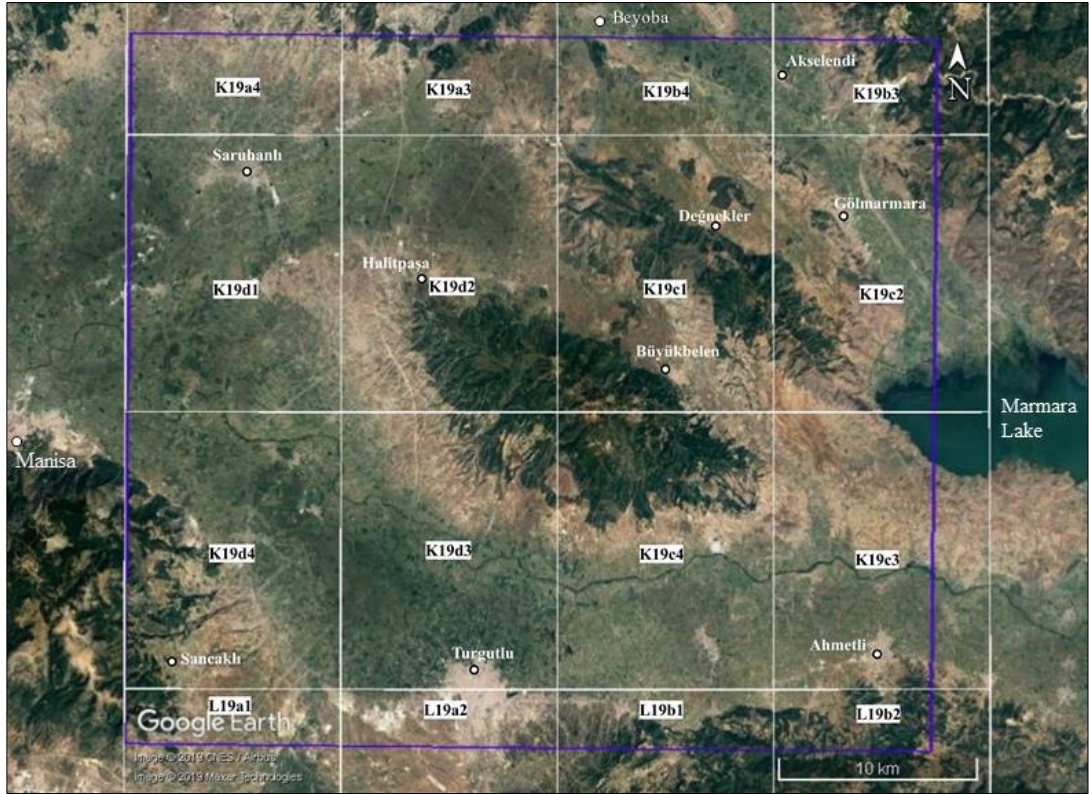


Figure 1.2. Geographic setting of the study area.

## 1.3. Method of Study

The study was conducted in three stages which are literature review, field studies and office works.

The GAG was examined by several researchers and the several geological studies were still continued in the region. Because previous studies on the region will help to

understand the evaluation and characteristics of the region, firstly the literature review was conducted.

The second stage for thesis is field works. During field works mainly faults were identified and examined. By using their slickenlines and field observations, types of the faults were determined. Numerous dip-strike measurements from the faults located within the study area were collected for kinematic analysis. Also, the dip-strike measurements from the bedding planes were collected for structural analysis.

Office works which is the last stage constitutes the most important of the thesis. At this stage, the study and evaluation of the methods to be applied in the softwares came to the fore. The measurements obtained in the field for structural and kinematic analyzes were evaluated by using different softwares. Rose diagrams were created for the strike measurements at 10° class intervals by using *Rockworks/15* software in order to analyse the attitude of the bedding and the fault planes. The slip-data measurements for the kinematic analysis were evaluated by using *TENSOR software* developed by Delvaux (1993). This program was used in order to understand principal paleo-stress directions of the faults.

Morphometry was used to measure the landscape shape quantitatively by using geomorphic indices which are useful in order to determine the tectonic activity level of the area. In this study, the asymmetry along ridges were studied by drawing several topographic profiles for three mountain ridges. In order to evaluate the slope changes of ridges, by using *ArcGIS 10.4.1 software* two slope maps were created according to degree changes and percentage changes, but they were proper for the purpose of the study. The software takes into account the stream channels and this causes information pollution. That is why by drawing several topographic profiles the slope changes were determined and the slope change map was created by correlating same slope intervals. That will be discussed in Chapter 4. By using the Smf index, the tectonic activity of the region was determined at three locations that are along the Manisa Fault, along the Gölarmara Fault, and along the northeast margin of Çaldağ.

## 1.4. Previous Studies

Previous studies can be divided into three main groups in terms of regional tectonic settings of the Aegean region, the tectonic evolution of the GAG, and the morphotectonic studies conducted near the study area and the GAG.

### 1.4.1. Regional Tectonic Settings

Turkey is a part of the Alpine-Himalayan belt with seismic activity at the junction of African, Eurasian and Arabian plates (Dewey & Şengör, 1979) (Figure 1.3). High seismic activity and complex deformation features have formed. Each plate has different effects on the creation of Anatolia because of the interaction and relative motion of these plates.

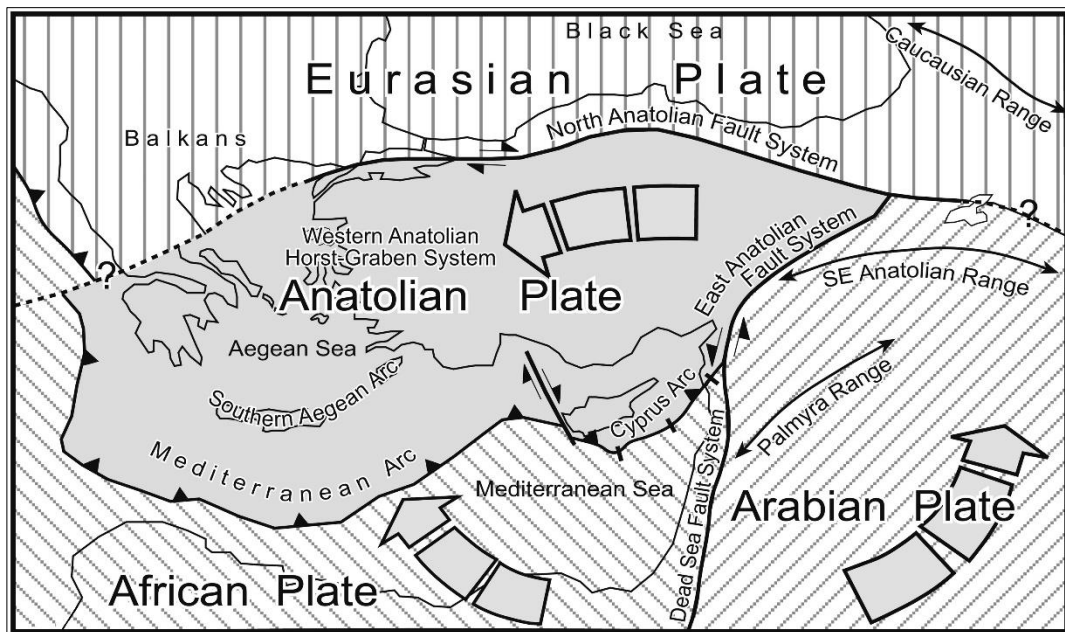


Figure 1.3. Tectonic setting of eastern Mediterranean (Bozkurt & Rojay, 2005).

Dewey and Şengör (1979) mentioned that the broad framework of the Aegean, Turkey and the eastern Mediterranean region is under the control of the Anatolian plate. The plate has rapid westward motion relative to the Eurasian plate whereas it has west-southwestward motion relative to the African plate. The Anatolian plate is moving into the western Mediterranean oceanic tract in west direction. The movement of the

plate with respect to Africa is taken up by subduction at the Aegean Trench. Because of the collision of both Arabian and Anatolian plates, the northern and eastern Anatolian transform faults have developed (Şengör & Yılmaz, 1981). The neotectonics of Turkey is under the control of three major elements; the Aegean-Cyprean Arc, the dextral North Anatolian Fault Zone and the sinistral East Anatolian Fault Zone. They have formed following the collisions of the plates. The Aegean-Cyprean Arc is the convergent plate boundary between the African and Anatolian plates. At this boundary the African plate is subducting beneath the Anatolian plate.

Global Positioning System (GPS) studies were conducted to understand relative timing of the motion of Arabian, African and Eurasian plates. The Arabian and African plates have relative motion to the Eurasian plate. McKenzie (1978) mentioned that the relative motion between Turkey which means Anatolia and Eurasia has been estimated as 4 mm/yr in an E-W direction in Western Anatolia. Reilinger et al. (1997) mentioned that the movement of the Arabian plate is at a rate of 25 mm/yr relative to the Eurasian plate in north-northwest direction. However, Kahle et al. (1998) determined the rate as 15 mm/yr relative to the Eurasia in the north direction. In addition to these relative motion rates, according to McClusky et al. (2000), the Arabian plate is moving at a rate of 18-25 mm/yr relative to the Eurasian plate in north-northwest direction. Reilinger et al. (1997) has determined that the movement of the African plate is at a rate of approximately 15 mm/yr. Also, Reilinger et al. (1997) and McClusky et al. (2000) defined same movement rate which is 10 mm/yr for the African plate relative to the Eurasia. According to the velocity difference between African and Arabian plates which is approximately 10-15 mm/yr, the Dead Sea transform fault has a left lateral characteristic (McClusky et al., 2000).

The interaction of African, Arabian and Eurasian plates shaped the Aegean Extensional Province (AEP) and as a result of the collision of African and Eurasian plates, a region of extensional deformation was formed. McKenzie (1978) and Şengör (1978) determined the total amount of extension in the Aegean but they estimated

different results. The overall expansion amount in the Aegean was estimated by McKenzie (1978) to be around 50%. However, according to Şengör (1978) this amount was estimated as 30%.

The reason of the neotectonic extension in western Anatolia is still debatable and many studies were conducted to understand this extension. Bozkurt (2001) gathered and examined all studies and as it mentioned in his study four different models were determined to explain the cause and origin of crustal extension in the Aegean. The models indicate different time intervals for commencement of extension in western Anatolia. These models are (a) Tectonic escape Model, (b) Back-arc spreading model, (c) Orogenic collapse model and (d) Episodic two-stage graben model.

*Tectonic escape model* is explained by the westward escaping of the Anatolian block from the east Anatolian zone along the North Anatolian and East Anatolian strike-slip faults due to Arabia-Eurasia collision since the Late Serravallian (~12 Ma) (Dewey & Şengör, 1979; Şengör et al., 1985; Şengör, 1987). According to Seyitoğlu and Scott (1996a), the time of the extensional tectonics in N-S direction was determined as latest Oligocene-Early Miocene in western Turkey. However, this cannot be explained by the tectonic escape model namely the collision of Arabia-Eurasia. Koçyiğit et al. (1999) mentioned that the escape of the Anatolian plate begun after the formation of the North Anatolian and East Anatolian fault system which were formed in Early Quaternary.

*Back-arc spreading model* was determined as the south-southwestward migration of the Aegean trench system and resulting west Anatolian extension (McKenzie, 1978; Le Pichon & Angelier, 1979). While Le Pichon and Angelier (1979) determined the time of subduction as 13 Ma, McKenzie (1978) mentioned the time of subduction as 5 Ma. In addition to them, Meulenkamp et al. (1988) suggested the subduction time as least 26 Ma. South-southwestward movement of the Aegean trench system was determined as the reason of the extensional evolution of the horst-graben system in back-arc spreading model (Koçyiğit et al., 1999).

*Orogenic collapse model* which started during the latest Oligocene-Early Miocene after the latest Paleocene was defined as the spreading and thinning of over-thickened crust (Seyitoglu & Scott, 1991; Seyitoğlu & Scott, 1992).

*Episodic two-stage graben model* was suggested as the model consists of the combination of the orogenic collapse model occurred along the İzmir-Ankara-Erzincan suture zone (a Miocene-Early Pliocene first stage) and tectonic escape model (a Plio-Quaternary second stage). The formations of the almost all grabens located in western Turkey are directly related with episodic two-stage graben model (Koçyiğit et al. 1999; Bozkurt & Rojay, 2005).

#### **1.4.2. The Gediz Alaşehir Graben (GAG)**

There are many east-west oriented and seismically active grabens in western Turkey. Some of the grabens located within the western Anatolia are Edremit, Kütahya, Bakırçay, Simav, Gediz Alaşehir, Büyük Menderes and Küçük Menderes (Figure 1.1).

As mentioned above, the one of the major grabens which is the seismically active is the GAG. The GAG starts at Alaşehir and extends to Manisa in the west (Figure 1.4). The length of the graben is approximately 150 km with a 15 km width around Salihli, and towards the western part, the width of the graben increases where the river plain merges with the Manisa-Akhisar-Soma basin. The graben shows NW- SE trending between Alaşehir and Salihli whereas the trend is in E-W and ENE-WSW direction between Salihli and Turgutlu.

The GAG which is divided into sub-grabens and horsts by the bifurcation of northern and southern graben bounding faults is extending in west direction.

The Gediz Alaşehir Graben (GAG) was subjected to many studies in terms of geology, tectonic evolution, structural geology and mineral deposits.

Emre (1996) studied the field observations about the relationship between top and bottom block and the Karadut Detachment Fault and tectonic evolution of graben.

According to the findings of study, the opening of the GAG starts with the formation of the Karadut Fault.

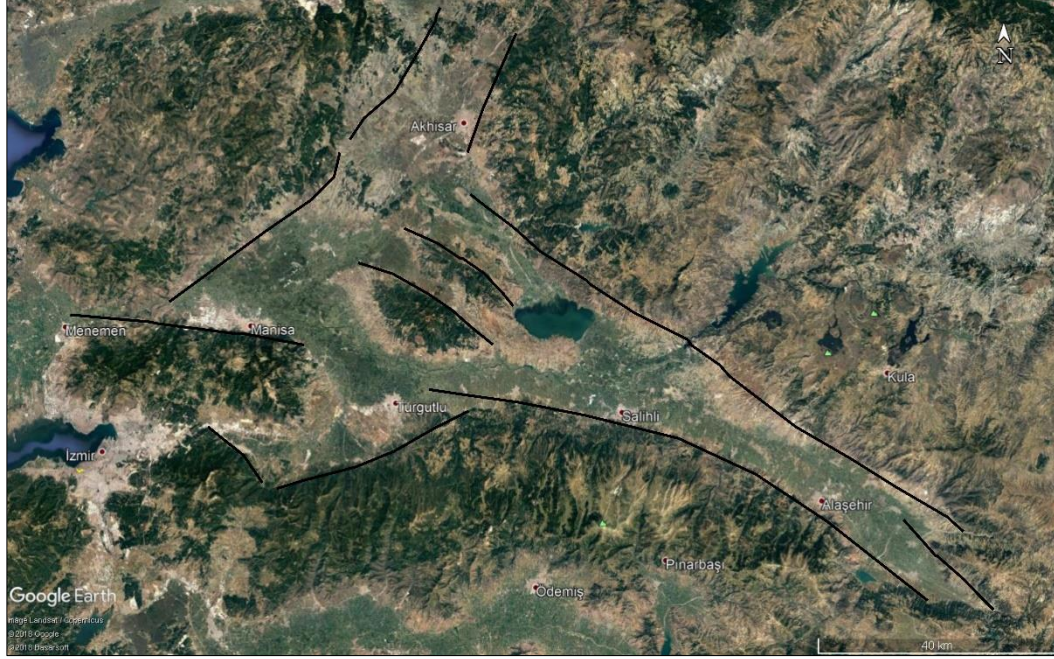


*Figure 1.4. Geographic setting of the Gediz Alaşehir Graben.*

Temiz et al. (1998) studied a detailed kinematic analysis of minor and major faults in lower Pliocene and Quaternary sediments which deposited on the southern margin of the GAG. According to the field observations, the kinematic analysis of faults give dominantly NNE-SSW extension.

Koçyiğit et al. (1999) mentioned that the graben has two sequences; Salihli Group (characterized by a Miocene-lower Pliocene continental sedimentary units) and Karataş Group (characterized by a Plio-Quaternary continental unit including alkali olivine basalts). The younger sequence is separated from the underlying, is assumed to be initially faulted and folded sequence by angular unconformably. This angular unconformity shows the evidence of the episodic two stage extensional model about the evolution of the GAG in western Anatolia.

Sözbilir (2001) studied the footwall and hanging-wall of the Gediz Detachment Fault which was also named as the Karadut Detachment Fault by Emre (1996) in terms of the geometric of macroscopic features such as folds and back-tilted strata.

Seyitoğlu et al. (2002) studied the tectonic development of the E-W trending GAG and the flexural rotation/rolling hinge model. Three fault systems were identified and at first fault system, there was an activity responsible for the accumulation of sedimentary units. A second fault system developed in the hanging-wall of the first system in Pliocene. Finally, the third fault system which is recently active separates older graben fill and sedimentary units.

Sarıkaya (2004) studied the field observations about the Gediz Detachment Fault and the petrographic analysis of the samples collected from this fault. In this context, according to the field and petrographic observations, the stratigraphy of the rock units which are under the effect of detachment fault was identified.

Bozkurt and Sözbilir (2006) studied the mechanisms of the Manisa Fault that are responsible for large-scale normal fault growth. Also, the stress field orientation was estimated by using inversion of fault scarp data. Thus, the kinematic evolution and development of the Manisa Fault were evaluated.

Çiftçi and Bozkurt (2007) studied the relay ramp formation as an example in the southern margin of the GAG according to morphological and structural feature of the relay ramp.

Özkaymak and Sözbilir (2008) studied the stratigraphic and structural evidence of fault reactivation related to the evolution of the western part of the Manisa Fault.

Çiftçi and Bozkurt (2009a) studied the hanging-wall deformation of the fault systems that were controlling the southern margin of the Gediz Alaşehir Graben in terms of geometry. The strike orientations of fault sets were identified predominantly around WNW-ESE.

Çiftçi and Bozkurt (2009b) studied the depositional history of the GAG by the field observations and the subsurface data. The study was focused on the Miocene sequences that were accumulated during the core-complex formation. The rate of structural controls on the evolution of the basin fill was explained according to sedimentological data.

Helvacı et al. (2013) studied the geology, mineralogy, geochemistry and formation phases of Ni-Co deposits of Çaldağ. Moreover, the fault types which are thrust, normal, and strike-slip faults were identified around Çaldağ region. The normal fault structures developed in NW-SE trending around Çaldağ, and they continue to form horst-graben structures to the north of Gölarmara.

Özkaymak et al. (2013) studied the western and northern margins of the Manisa Basin in terms of structural features and kinematic analyses. Outcrop-scale faults and their kinematic features were evaluated to analyze the basin. Four main structures that are reverse faults, normal faults, strike-slip faults, and folds were identified.

Kent et al. (2016) studied previously published datasets were combined by digital elevation model to obtain fault throw and slip rate from cross sections that are geologically well-constrained, and these data were estimated to evaluate fault throw rate across the southern margin of the GAG by using topographic metrics. Thus, the important information about the active tectonics of the GAG, future seismic hazard and risk analyzes were provided by these new data. The total throw on the normal faults were determined approximately 2000 m to 3900 m between the Bozdağ Fault and GAG Boundary Fault.

Kent et al. (2017) studied new limitations on the fault slip rates and landscape response times of the GAG. The evolution of the south of the GAG from the Pliocene to recent was evaluated and also, the relationship between active faulting and the fluvial system was researched.

### 1.4.3. Morphometric Studies

Süzen et al. (2006) studied high-altitude Plio(?)–Quaternary fluvial units deposited over the Bozdağ horst in terms of the origin and regional tectonic implications. The Bozdağ horst which is the southern margin of the GAG, is defined as an important structure developed within the horst-graben system of western Anatolia. By using lithological characterization, age, and deformation features of the region with morphological properties, it was aimed to identify the geometry, pattern, and evolution of Plio(?)–Quaternary deposits with respect to recent tectonic activity in western Anatolia. According to geological and geomorphological investigations, a four-stage evolutionary model was identified for the deposits. By considering this model, the amount of tilting was estimated as  $1.2^{\circ}$  to  $2.2^{\circ}$ . The age of tilting is presumed to be Plio–Quaternary according to the timing of rifting in the region and the age of the fills in the elevated lakes.

Özkaymak and Sözbilir (2012) studied the Spil Mountain which is known as the footwall block of the Manisa Fault Zone (MFZ). A detailed geomorphic study of the fault generated mountain fronts and drainage pattern of the Spil Mountain were determined by using morphometric indices. The oxbow formations within the study area were observed and this has indicated that the modern channel of the Gediz River migrated. This suggests the southwestward back tilting of the basin floor. The mountain front sinuosity (Smf) results show tectonically active mountain front in western (1.11–1.14), eastern (1.12) and central parts (1.12–1.14). The valley floor width-to-height ratio (Vf) values are high in the western and eastern of the mountain front whereas the Vf value is low in the central mountain front. The results of the Vf values indicate that there is an active uplift in the Spil Mountain. Thus, all results have shown that there is a high degree of tectonic activity along the MFZ. Özkaymak et al. (2011) mentioned the uplift rate of Manisa Fault Zone as 0.1–0.3 mm/yr.

Özkaymak (2015) studied the Honaz Fault which is the southern margin of the Denizli Graben Horst System in the western Anatolia in order to understand the kinematic

analysis of the fault by using geomorphic indices. According to obtained Smf value which is 1.14, it can be understood that the region is tectonically active. By evaluating the oxbow lakes formed in the region, the river migration was determined. According to the locations of paleochannels and the modern channel of the river, it was observed that there is the southward black-tilting of the basin floor. The Vf values are low in the mountain front and this shows that there is an active uplift in the region. The AF values which are between 47-82 have been categorized in three parts according to AF results, and the calculations have shown dominantly asymmetric patterns in the region. Only at three calculation parts, the AF values were calculated as 50, and this indicates symmetry in the region. Thus, all results obtained from geomorphic indices shows high degree of tectonic activity along the Honaz Fault. The minimum slip rates of the Honaz Fault was determined as 0.15-0.38 mm/yr.

Tepe and Sözbilir (2017) studied the Kemalpaşa Basin and surrounding horsts located at southwestern part of the GAG in terms of tectonic geomorphology. The Kemalpaşa Basin is under the influence of the Kemalpaşa Fault and a number of downstepping faults known as Spildağı Fault Zone. By using geomorphic indices, the tectonic activities of these faults was studied. The Smf in the north side was calculated as 1.29, 1.32, and 1.56 respectively from west to east. The Smf in the south side was calculated as 1.12, 1.14, 1.25, and 1.30. The Smf values of both sides indicate the active fronts and facet slopes implied a relatively high degree of activity along the both sides of the Kemalpaşa Basin. The Vf values are less than 1 for both sides of the basin and this indicated tectonically active mountain fronts. All morphometric results suggested that both sides of the Kemalpaşa Fault are tectonically active. The uplift rate for the Kemalpaşa Basin was not been determined in this study. Tepe and Sözbilir (2017) mentioned from Özkaymak et al. (2011) that the minimum slip rates for the different sectors of Manisa Fault Zone (MFZ) was determined about 0.1-0.3 mm/yr.

Topal and Özkul (2018) studied relative tectonic activity of the Honaz Fault by using geomorphic indices. The Honaz Fault formed from two segments that are the Karateke and Honaz. The indices were applied for these segments separately. The Smf values

show that the study area is significantly active. The AF was calculated for both segments, and the results indicated that the Honaz Segment is tilting towards the west whereas the Karateke segment has irregularity.

Topal (2019a) studied the Karacasu Basin cutting obliquely the Büyük Menderes Graben in terms of tectonic activity by using geomorphic indices. The Karacasu Fault was divided into two segments that are Çamköy and Yazır. The geomorphic indices were conducted for both segments. The Smf values were calculated as 1.51, 1.52, 1.72, and 2.51 at four drainage basins. The Vf values are between 0.21 and 1.07 at seventeen drainage basins. By using Smf and Vf values, the uplift rates of Çamköy and Yazır segments was determined as 0.05-0.5 mm/yr.

Topal (2019b) studied the Priene-Sazlı Fault located at the Söke Basin, and this basin is the west part of the Büyük Menderes Graben with NE-SW trending. The aim of the study is to evaluate the tectonic activity of the fault and the morphotectonic evolution of the region. Geomorphic indices were used in this context. The AF values are between 0.23 and 0.76 at 37 drainage basins, and these indicate that there is an asymmetry. The Smf value was calculated as 1.15, 1.16, 1.26, 1.30, 1.42, 1.60, and 1.96 at eight drainage basins. The Vf values are between 0.27 and 1.66 at 37 drainage basins. According to the results obtained from the Smf and the Vf, the uplift rate in the region was determined as 0.05 mm/yr.

## CHAPTER 2

### STRATIGRAPHY

The aim of this chapter is to give an information on relative dating of the faults that are analyzed especially in morphometric analysis. The rock units were divided into two main groups which are pre-Miocene sequence accepted as the basement of Neogene basins and Miocene to Quaternary sequences in the Gediz area (Erdoğan, 1990) (Figure 2.1, Figure 2.2). The basement includes several rock units that are Menderes metamorphics, Cretaceous Ophiolitic Accretionary Complex, Cretaceous-Paleogene Bornova flysch, and Eocene Marine sequences (Figure 2.3). Only the Cretaceous ophiolitic mélange and Bornova flysch were observed within the study area. Neogene rocks units was classified as the Miocene sequence and the Pliocene sequence in this study. Quaternary units consist of the travertine, talus deposits, alluvial fans, terrace conglomerates and alluvium (Figure 2.3).

The Miocene sequence is generally observed at foot of the Spil Mountain, at south of Turgutlu-Ahmetli, and at all around the Çaldağ (Figure 2.1). The sequence unconformably overlies the basement. The Miocene sequence consists of red clastics which are laterally and vertically grading to andesitic volcanics, mudrocks, clayey limestones and lacustrine deposits to the top. An unconformable boundary between Early Miocene red clastics-clayey limestones and Late Miocene lacustrine deposits is recorded locally.

The Pliocene sequence includes continental clastics, and there is an unconformity with Miocene sequences. The Pliocene sequence is generally characterized by conglomerate, sandstone and mudstone with cross-bedded sandy layers and river channel deposits. Over this unit, unconformably Quaternary units are deposited.

Quaternary units are widely seen in the study area and cover more than half of the region. The units can be classified into sub-units that are talus/fan deposits, sand dunes, recent alluvium and travertine. Talus to fan deposits generally are observed at where the faults link to the high topographic elevations. Talus deposits are observed mostly at steep slopes consist of angular to sub-angular pebbles with no internal structure. Alluvial fan deposits observed at gentle slopes and at some locations successive fan deposition is still observed. The most typical examples of the fans are observed at southeast of Spil Mountain, along the Turgutlu-Ahmetli margin and the southern margin of Çaldağ (Figure 2.1). Quaternary fill-deposits of Gediz basin forms recent alluvial deposit within the region.

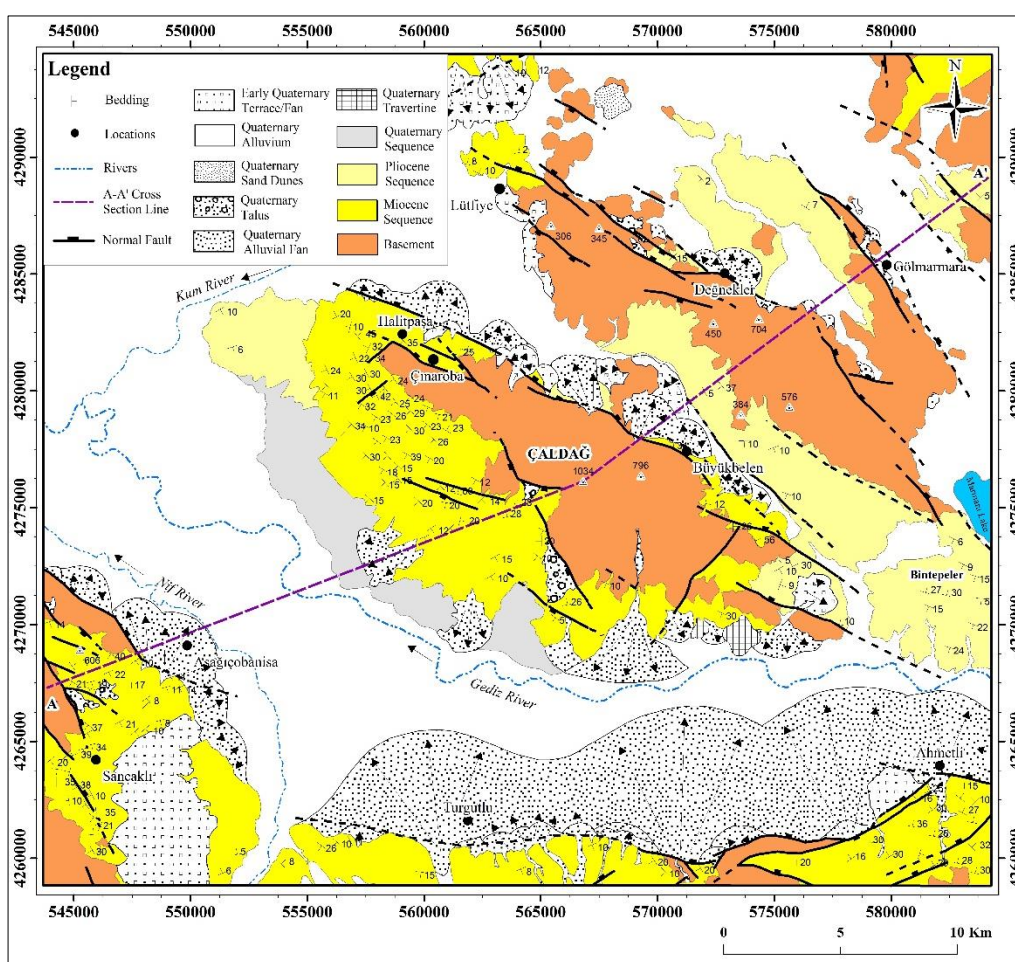


Figure 2.1. Generalized geological map of the study area (partially compiled from Rojay and Toprak, 2001).

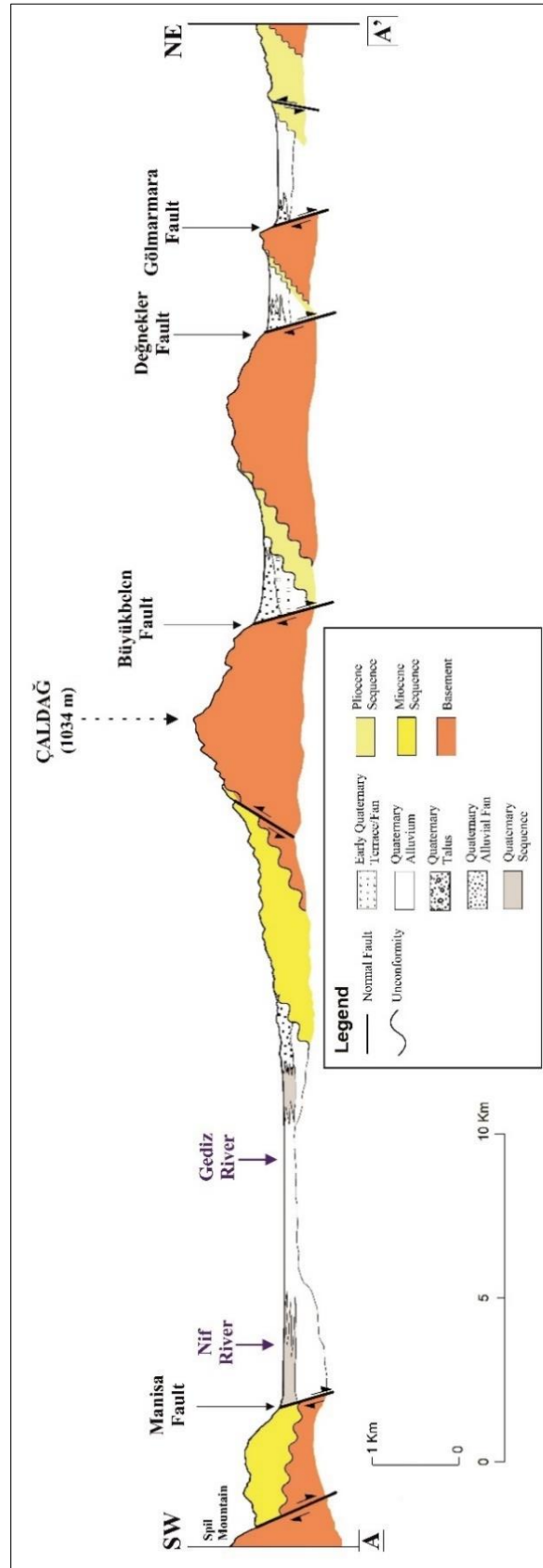


Figure 2.2. A-A' Cross Section along the study area.

Moreover, travertine formation is observed at southeastern side of the Çaldağ, in Canbazlı and Harmandalı villages. Sand dunes are observed to the northwest of the Değnekler, around south of Sazoba (Figure 2.1).

AGE	LITHOLOGY	DESCRIPTION	UNIT
Quat. 2.6 Ma		Alluvium, Alluvial Fans, Talus, Terrace Conglomerates and Travertine	Quat. Seq.
Pliocene 5.4 Ma		Fluvial Clastics	Pliocene Sequence
Late Miocene 12 Ma		Red clastics (along the margins) to Lacustrine sequences (to the depocenters)	Miocene Sequence
Oligocene(?) - Early Miocene 23 Ma		Alternation of beige to white Mudrocks, clayey limestones  Red clastics (Conglomerates-Sandstones) Andesitic Volcanics (CA lavas, ignimbrites, pyroclastics)	
Pre-Miocene		Unconformity Eocene Marine Sequence Cretaceous Ophiolitic Accretionary Complex Cretaceous-Paleogene Bornava Flysch Menderes Metamorphic Complex	Basement

Figure 2.3. Generalized tectono-stratigraphic columnar section of the study area; not to scale (Ages are from International Commission on Stratigraphy).

## CHAPTER 3

### STRUCTURAL GEOLOGY

The chapter is divided into three main parts; attitude of bedding planes, attitude of faults, and kinematic analysis of faults. In the bedding attitude part, the general trend of the Miocene and Pliocene sequences will be evaluated. In the fault attitude part, the general trend of faults will be evaluated with a length weighted rose diagram. In kinematic analysis part, the faults whose strike, dip, and slickenlines were measured in the field will be studied in terms of stress tensor.

#### **3.1. Attitude of the Bedding Planes**

174 dip-strike measurements of the bedding plane were taken from the Pliocene and the Miocene sequences (Figure 2.1). While 26 dip-strike measurements are from the Pliocene sequence, the remaining measurements are measured from the Miocene sequence. The rose diagram was prepared by using *Rockworks* software, to understand the general trend of the bedding planes. The rose diagram of the Pliocene sequences show that the most prominent strike trend is between 100°N and 120°N (WNW-ESE) (Figure 3.1). Dip measurements show that the range is between 05° and 37°. The direction of dip generally is in SW direction in the Pliocene sequence. 148 measurements out of 174 were measured from the Miocene sequence. The rose diagram shows that the most prominent strike trend is 120°N-140°N (NW-SE), and the second most prominent strike trend is 60°N-80°N (ENE-WSW) (Figure 3.2). Dip measurements of the Miocene sequence indicate that the range is between 05° and 60°. The general dip direction of this sequence is SW.

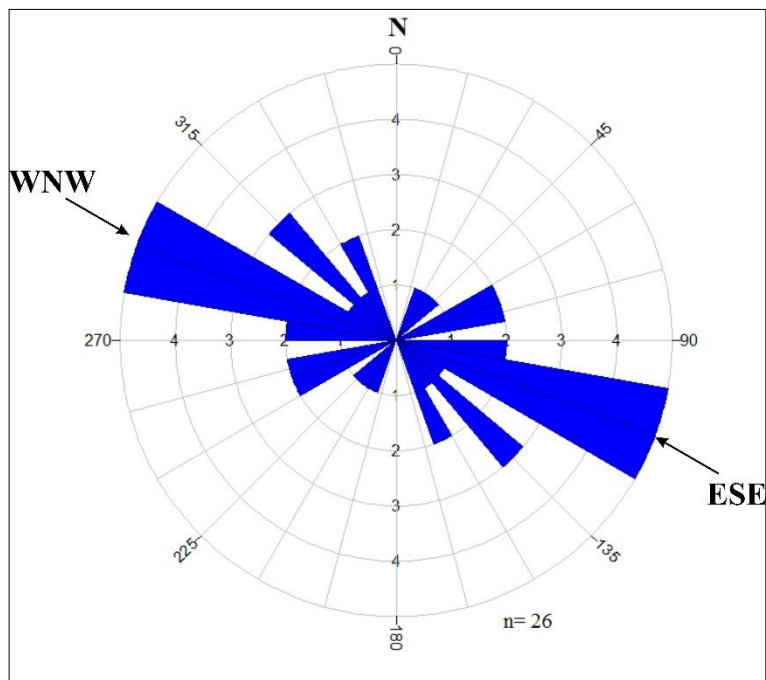


Figure 3.1. The rose diagram showing strike measurements taken from the bedding planes of the Pliocene sequences (n= 26).

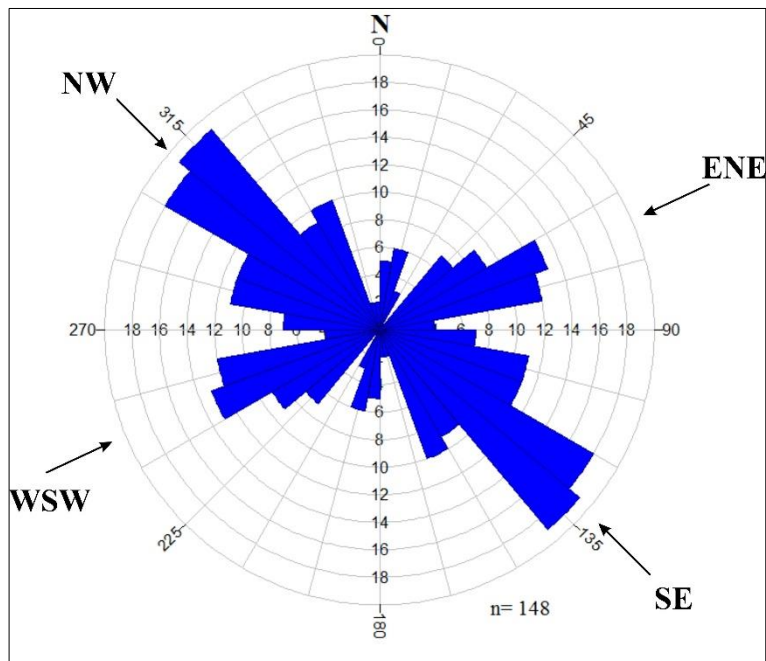


Figure 3.2. The rose diagram showing strike measurements taken from the bedding planes of the Miocene sequence (n= 148).

### 3.2. Attitude of the Faults

In this part, a length weighted rose diagram of the strike of faults was prepared to understand the dominant trend of the faults within the study area (Figure 3.3). By measuring the length and the strike of the faults drawn in the geological map view, all measurement was noted. During the measurement, the important point is the changes in the trend of the faults, knick points along the faults and the length between these changes. The most prominent strike trend is  $120^{\circ}\text{N}-130^{\circ}\text{N}$  (ESE-WNW), the second prominent trend is  $140^{\circ}\text{N}-150^{\circ}\text{N}$  (NNW-SSE), and the third prominent strike is  $50^{\circ}\text{N}-70^{\circ}\text{N}$  (ENE-WSW) (Figure 3.3). This means that the fault elongation is generally in NW-SE direction within the study area.

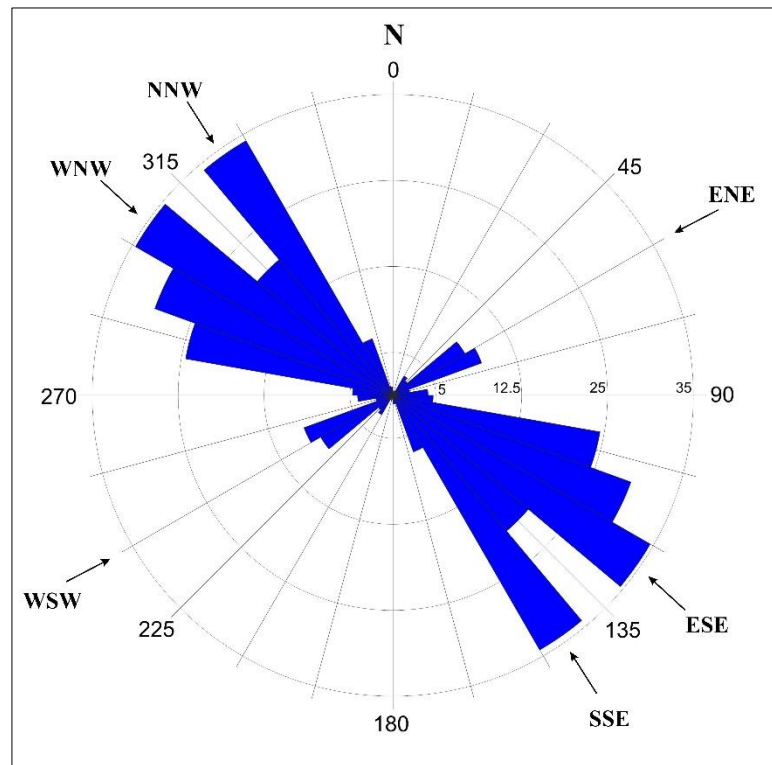


Figure 3.3. The length weighted rose diagram of the faults showing the general trend within the study area. (The total number of recorded faults is 100 and total length is 189.3 cm in map scale).

### 3.3. Kinematic Analysis of the Faults

By measuring data from the fault plane markings in the study area, both the deformation characteristics of the region and the geometry of the fault systems are tried to evaluate. The strike, dip, and rake of the slickenlines of the fault planes are measured to understand the fault kinematics in the region. By using fault slip-data, the four parameters of the reduced stress tensor are obtained. These parameters are obtained by an improved version of the right dihedral method (Angelier & Mechler, 1977) and rotational optimization method by using the *TENSOR* software developed by Delvaux (1993). The four parameters were defined as  $\sigma_1$  (maximum stress),  $\sigma_2$  (intermediate stress),  $\sigma_3$  (minimum stress), and R (the ratio of principal stress differences). The ratio is calculated by using a formula which is  $R = (\sigma_2 - \sigma_3) / (\sigma_1 - \sigma_3)$ . The type of stress tensor is defined by stress regime, and Delvaux et al. (1997) used stress regime term to identify the type of stress acting in his study area. The nature of the vertical stress axes helps to the determination of stress regime which means that if  $\sigma_1$  is vertical, the stress regime is extensional, if  $\sigma_2$  is vertical, the stress regime is strike-slip, and if  $\sigma_3$  is vertical, the regime is compressional. Here, the relationship between  $\sigma_1$  and  $\sigma_3$  is the main evaluating tool. Also, the stress regime can be classified in itself according to the R-value (Figure 3.4). The orientation of principal stresses indicates the type of fault (Figure 3.5). If  $\sigma_1$  is vertical on stereoplot, the fault shows normal fault character. This condition also can be applied to other axes. If  $\sigma_2$  is vertical, the fault is strike-slip, and if  $\sigma_3$  is vertical, the fault is thrust.  $\sigma_1$  is vertical on circumstances which indicates a normal faulting in locations. According to the ratio results and the stress axes, the faults defined within the study area will be identified in terms of these parameters.

During the field study, totally 120 slip-data were measured from determined fault planes at different 8 locations. In this part, these slip-data are evaluated in terms of kinematic analysis, and the fault activity within the study area is understood. The principal stress values are mentioned in plunge and azimuth order in this study.

Stress Tensor Type	EXTENSIVE				STRIKE-SLIP				COMPRESSIVE				
Stress Symbols													
Stress Ratio R	0.00	0.25	0.50	0.75	1.00	0.75	0.50	0.25	0.00	0.25	0.50	0.75	1.00
Stress Regime	Radial EXTENSIVE	Pure EXTENSIVE	TRANS-TENSIVE	Pure STRIKE-SLIP	TRANS-PRESSIVE	Pure COMPRESSIVE	Pure COMPRESSIVE	TRANS-PRESSIVE	Pure STRIKE-SLIP	TRANS-TENSIVE	Pure EXTENSIVE	Radial COMPRESSIVE	Radial COMPRESSIVE

Figure 3.4. Illustration showing the stress tensor types, stress symbols, stress ratio values and stress regime definitions (modified from Delvaux et al., 1997).

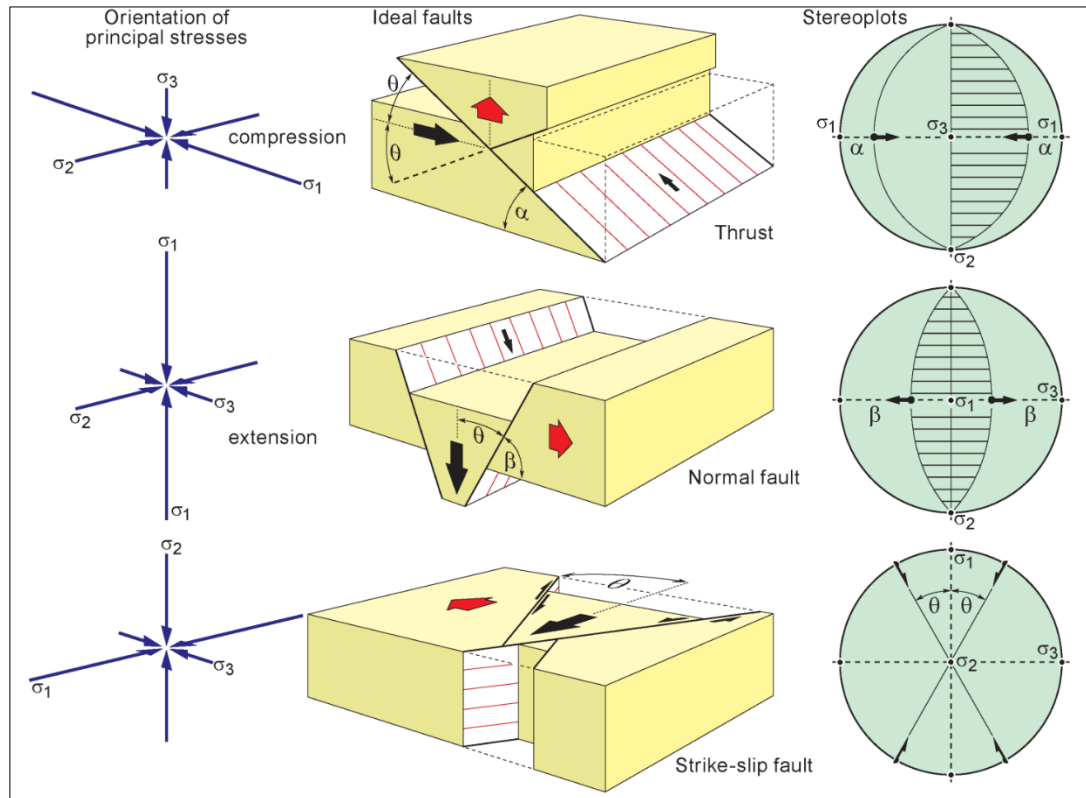


Figure 3.5. The principal stresses defining the fault type according to their orientation (Burg, 2017).

### 3.3.1. Çınaroba (Northwest of Çaldağ Ridge)

Çınaroba is located northwest of the Çaldağ Ridge (Figure 2.1). Within the Çınaroba area, the fault plane has strike values ranging from 300°N to 315°N, and these planes are dipping to 54°-62° northeast (Figure 3.6). 5 slip-data were measured from the fault plane, the principal stress axes and the ratio of principal stress differences were obtained for kinematic analysis.  $\sigma_1$  (maximum stress) is 75/257,  $\sigma_2$  (intermediate stress) is 11/123 and  $\sigma_3$  (minimum stress) is 11/031 (Figure 3.7). According to these results, the maximum stress value is almost vertical, and the fault obtained in Çınaroba has an extension in NE-SW direction. The R-value is 0.50 and as it can be understood from the table of the meaning of stress regime developed by Delvaux et al. (1997) (Figure 3.4), the fault has pure extension characteristic, and is a normal fault (Figure 3.5).



*Figure 3.6.* The fault plane studied in Çınaroba, Çaldağ has NW-SE trending with NE dipping (E: 559701, N: 4281354, Zone: 35).

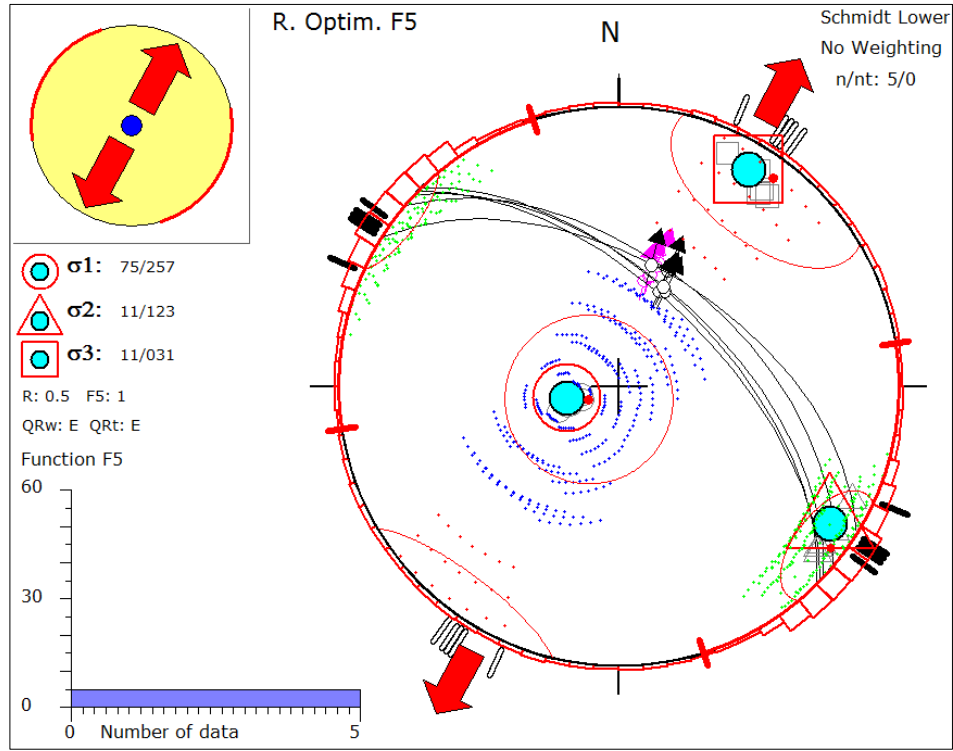


Figure 3.7. The principal stress axes of the fault in Çınaroba, Çaldağ.

### 3.3.2. Halitpaşa (Northwest of Çaldağ Ridge)

Halitpaşa is located northwest of the Çaldağ Ridge and also it is the neighbor with Çınaroba (Figure 2.1). The fault plane studied in Halitpaşa has 300°N-311°N trend, and dip of 30°-37° northeast (Figure 3.8). 4 slip-data were measured from the fault plane, the principal stress axes and the ratio of principal stress differences were obtained for kinematic analysis (Figure 3.9).  $\sigma_1$  (maximum stress) is 76/338,  $\sigma_2$  (intermediate stress) is 10/111, and  $\sigma_3$  (minimum stress) is 10/203. These results show that the maximum stress is almost vertical, and the fault experienced has an extension in NE-SW direction. The R-value is 0.50 and accordingly in Halitpaşa, the fault is a normal fault (Figure 3.5).



Figure 3.8. The fault plane studied in Halitpaşa, Çaldağ has NW-SE trending with NE dipping (E: 559705, N: 4281349, Zone: 35).

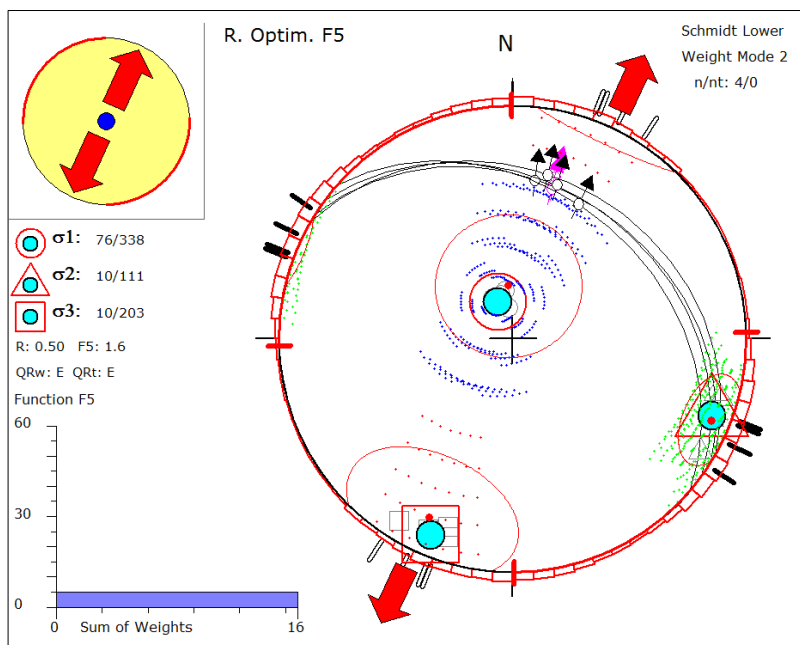


Figure 3.9. The principal stress axes of the fault in Halitpaşa, Çaldağ.

### 3.3.3. Değnekler (Değnekler Ridge)

Değnekler is located northside of the Değnekler Ridge (Figure 2.1). The fault plane studied in Değnekler has 315°N-319°N trend, and the plane is dipping to 32°-36° northeast (Figure 3.10). 4 slip-data were measured from the fault plane, the results of principal stress axes are  $\sigma_1$  (maximum stress) is 76/002,  $\sigma_2$  (intermediate stress) is 08/124, and  $\sigma_3$  (minimum stress) is 12/215 (Figure 3.11). According to these results, it can be determined that the maximum stress is almost vertical, and the fault obtained in Değnekler has NE-SW extension. The R-value is determined as 0.50. According to the ratio, the fault is a normal fault (Figure 3.5).



*Figure 3.10.* The fault plane studied in Değnekler has NW-SE trending with NE dipping (E: 572993, N: 4284830, Zone: 35).

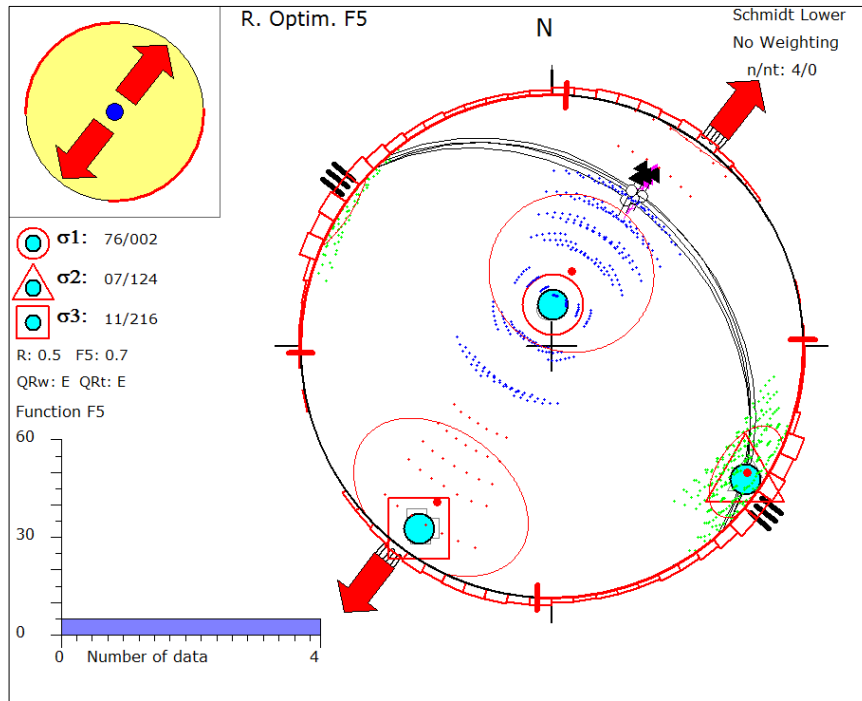


Figure 3.11. The principal stress axes of the fault in Değnekler.

### 3.3.4. Lütfiye (Northwest of Değnekler Ridge)

Lütfiye is located northwest of the Değnekler Ridge and the fault was determined within the abandoned quarry (Figure 2.1). The trend of the fault plane is between  $306^{\circ}\text{N}$  and  $322^{\circ}\text{N}$ . Moreover, the fault is dipping to  $60^{\circ}$ - $64^{\circ}$  northeast (Figure 3.12). The fault extends approximately 100 meters to the southeast from the measured point. 5 slip-data were measured from the fault plane. The results of principal stress axes are  $\sigma_1$  (maximum stress) is 67/257,  $\sigma_2$  (intermediate stress) is 17/121, and  $\sigma_3$  (minimum stress) is 15/027 (Figure 3.13). The maximum stress is almost vertical, and the fault evaluated in quarry has an extension in NE-SW direction. The R-value is 0.50, and the fault has pure extension characteristic (Figure 3.5) and it is a normal fault (Figure 3.6).



Figure 3.12. The fault plane studied in abandoned quarry located in the north of Lütfiye, Değnekler has NW-SE trending with NE dipping (E: 565072, N: 4288967, Zone: 35).

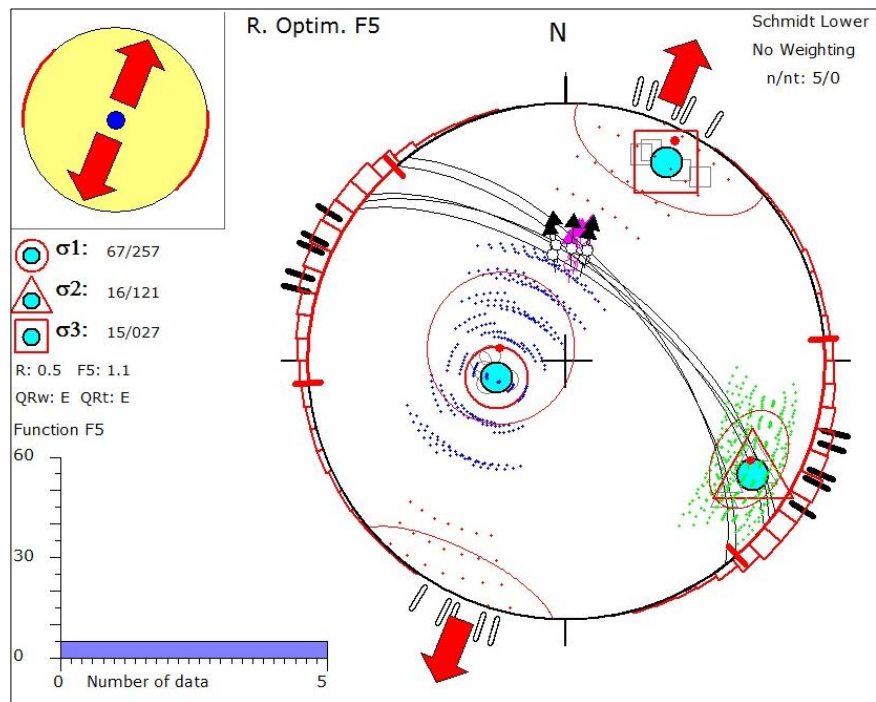


Figure 3.13. The principal stress axes of the fault in abandoned quarry located in the north of Lütfiye.

### 3.3.5. Gölarmara (Gölarmara Ridge)

Gölarmara is located at the northeast side of the Gölarmara Ridge (Figure 2.1). The fault plane studied in Gölarmara has 290°N-297°N trend, and the plane is dipping to 30°-36° northeast (Figure 3.14). 4 slip-data were measured from the fault plane. The results of principal stress axes are  $\sigma_1$  (maximum stress) is 76/352,  $\sigma_2$  (intermediate stress) is 06/106, and  $\sigma_3$  (minimum stress) is 13/197 (Figure 3.15). The maximum stress is almost vertical, and the fault has an extension in NE-SW direction. The ratio of principal stress differences (R) is determined as 0.50, and the fault has pure extension characteristic in terms of stress regime. Moreover, the fault is a normal fault due to the vertical  $\sigma_1$  (Figure 3.5).



*Figure 3.14.* The fault plane studied in Gölarmara has NW-SE trending with NE dipping (E: 579504, N: 4284677, Zone: 35).

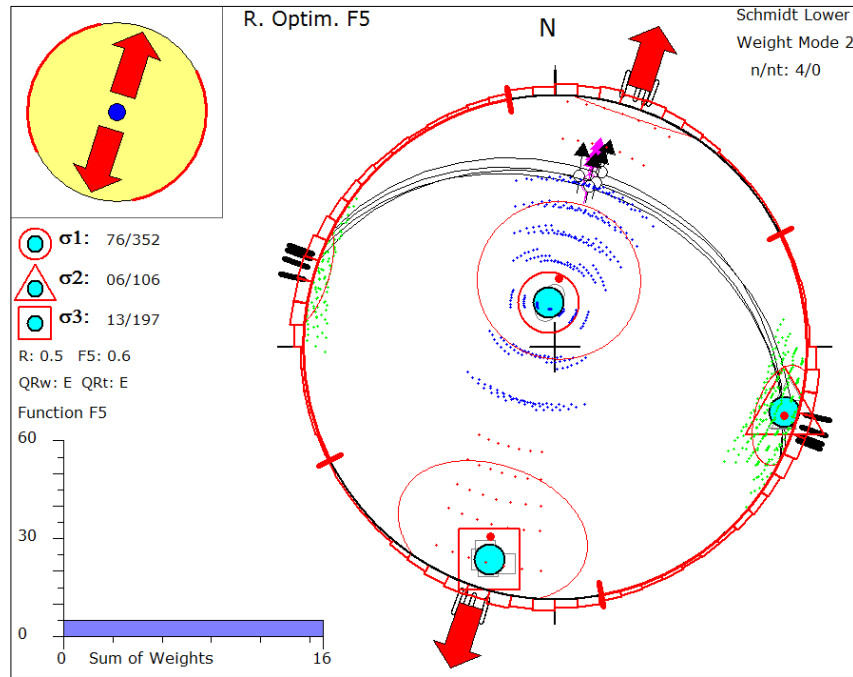


Figure 3.15. The principal stress axes of the fault in Gölarmara.

### 3.3.6. Sancaklıkayadibi (Spil Mountain)

Sancaklıkayadibi is located at the Spil Mountain in Manisa (Figure 2.1). During field study around Sancaklıkayadibi, two fault planes having different trend were observed. While the first fault plane has 346°N-351°N trend, the second fault plane has 323°-326°N trend. The dip amount of these planes is between 47° and 55° to northeast (Figure 3.16 and Figure 3.17). Each fault plane is exposed to erosion in the field. Totally 12 slip-data were measured from these fault planes and the kinematic analysis of these fault are evaluated separately.

8 measurements out of 12 were measured from the first fault plane. The results of principal axes are  $\sigma_1$  (maximum stress) is 72/326,  $\sigma_2$  (intermediate stress) is 18/150, and  $\sigma_3$  (minimum stress) is 01/059 (Figure 3.18). From other fault plane 4 slip-data were measured. Same as previous fault planes, the results of principal stress axes are determined.  $\sigma_1$  (maximum stress) is 72/287,  $\sigma_2$  (intermediate stress) is 16/133, and  $\sigma_3$  (minimum stress) is 07/041 (Figure 3.19). The maximum stress results of these faults indicate that the stress is almost vertical, and the fault evaluated in Sancaklıkayadibi

has an extension in NE-SW direction. The ratio of principal stress differences (R) was obtained as 0.50 for these two faults, and the faults have pure extension characteristic feature (Figure 3.5).



*Figure 3.16.* The first fault plane studied in Sancaklıkayadibi, Spil Mountain is 346°N-351°N trend with NE dipping (E: 545087, N: 4266406, Zone: 35).



*Figure 3.17.* The second fault plane obtained in Sancaklıkayadibi is 323°-326°N trend with NE dipping (E: 545136, N: 4266168, Zone: 35).

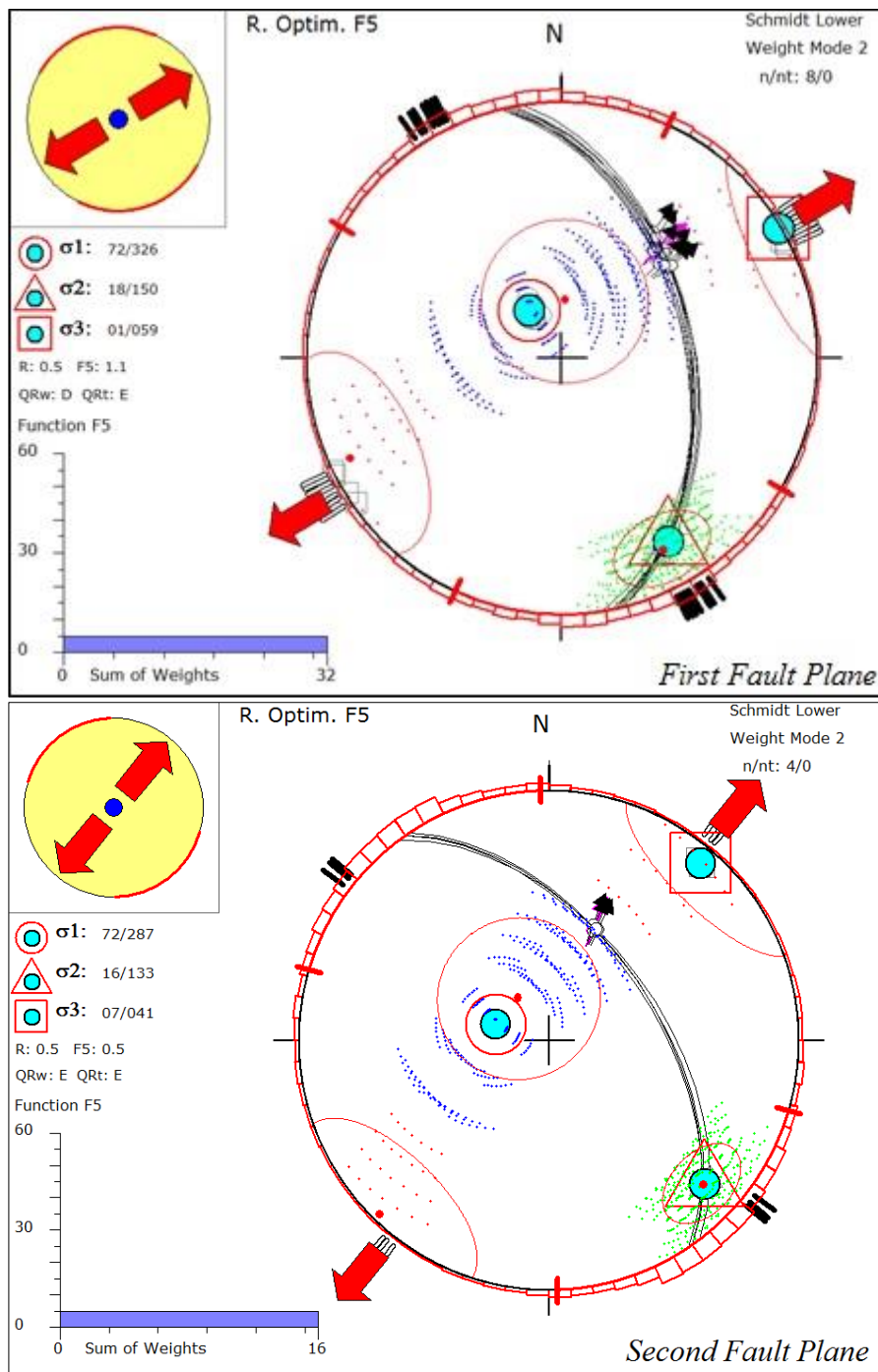


Figure 3.18. The principal stress axes of the all fault planes in Sancaklıkayadibi, Spil Mountain.

The fault trend is turning to the north, but it is not losing the characteristic feature at that point. For the fault planes, it can be said that because  $\sigma_1$  is vertical, the faults are a normal fault (Figure 3.19).

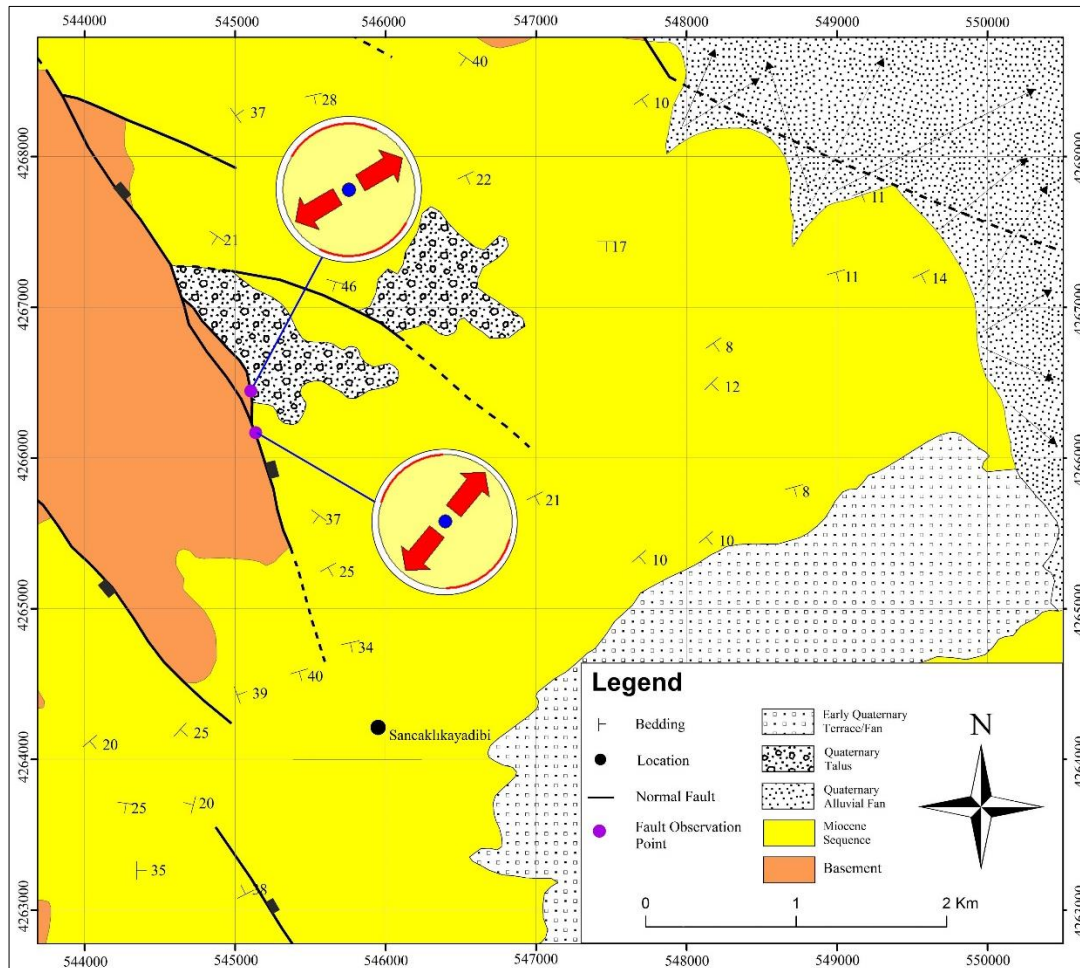


Figure 3.19. The faults studied in Sancaklıkayadibi, Spil Mountain have NE-SW extension. The fault located at north has  $346^{\circ}\text{N}-351^{\circ}\text{N}$  trend and the fault located at south has  $323^{\circ}-326^{\circ}\text{N}$  trend.

### 3.3.7. The Manisa Fault

The Manisa fault which is a 50-km-long is located between Manisa in the northwest and the GAG in the southeast. The fault is mainly in the NW trend and convex to NE. (Bozkurt & Sözbilir, 2006; Özkaymak & Sözbilir, 2008). The Manisa Fault was clearly observed along the Manisa-Turgutlu highway. At three locations along the highway, 49 slip-data were measured from the fault plane to determine the kinematic evolution of the fault. Three locations was evaluated in this part (Figure 3.20).

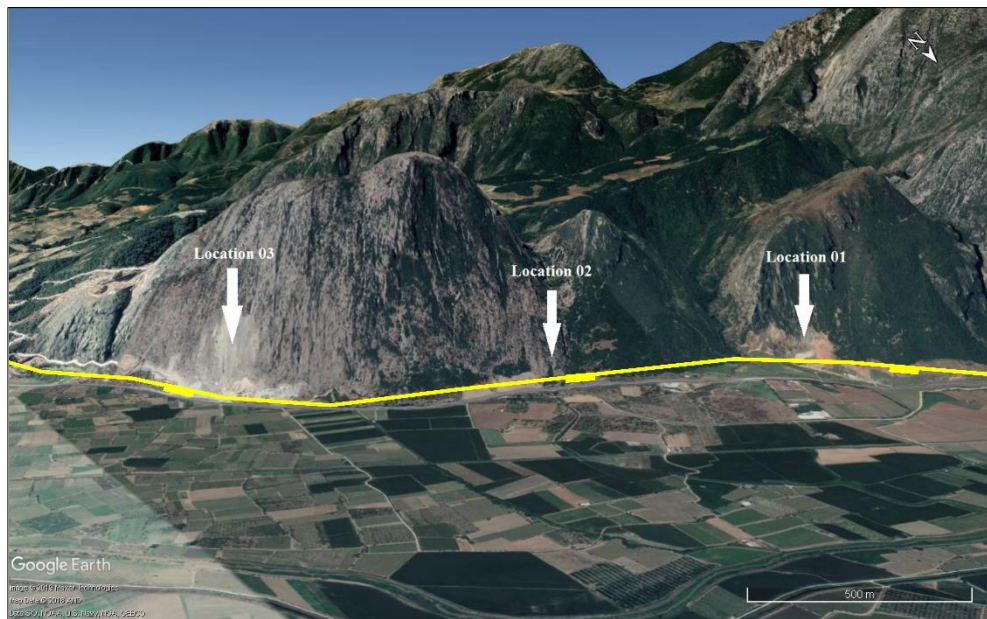


Figure 3.20. The locations where the slip-data have been collected and kinematic analysis has been studied along the Manisa Fault.

- Location 01 (Manisa Fault)

At Location 01, 14 slip-data measurements were collected from the fault plane divided into three parts. The general trend of the fault is  $285^{\circ}\text{N}$ - $297^{\circ}\text{N}$  for part A and C, but at one point, the trend is changing to  $310^{\circ}\text{N}$ - $318^{\circ}\text{N}$  at part B (Figure 3.21). That's why, the kinematic evolution will be studied on the fault plane separately. When all slip-data evaluated together, the principal stress axes and the ratio of principal stress axes differences are determined differently, and this does not reflect the reality for kinematic evolution.

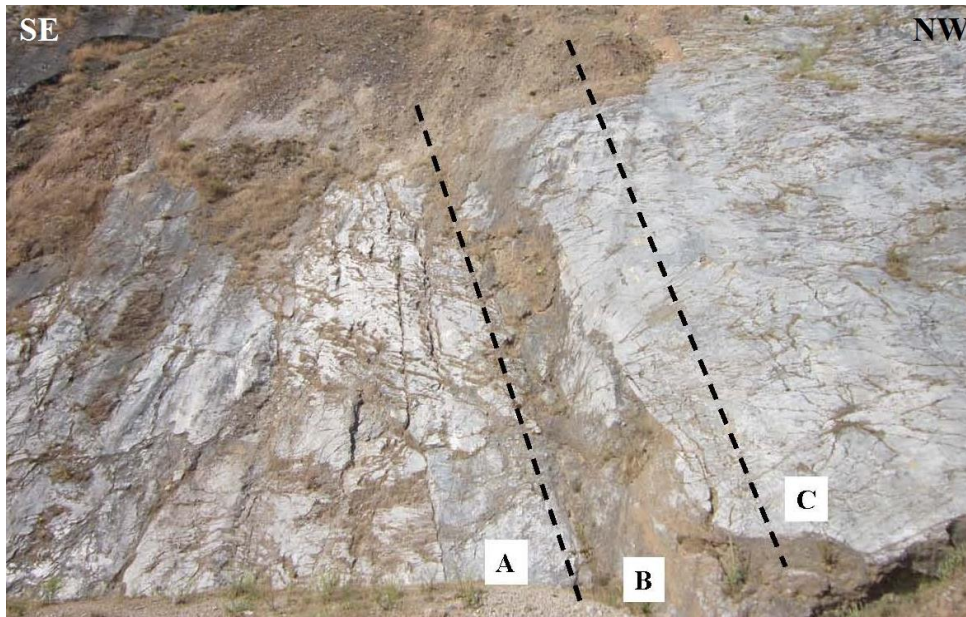


Figure 3.21. The fault plane showing three parts at Location 01 along the Manisa Fault (E: 544839, N: 4271464, Zone: 35).

The dip amount of the fault plane is varying in between  $45^\circ$  and  $50^\circ$  to northeast. The fault plane is divided into three parts in this location. the principal stress axes and the R-value were obtained for kinematic analysis (Table 3.1).

Table 3.1. The principal stress axes and the R-value results for the Manisa Fault at Location 01.

Part	$\sigma_1$		$\sigma_2$		$\sigma_3$		R
	Trend	Plunge	Trend	Plunge	Trend	Plunge	
A	272	71	089	19	179	01	0.50
B	301	78	122	12	032	00	0.50
C	286	77	103	13	193	01	0.50

The operating extension on parts shows different directions. For part A, the extension is in N-S direction, for part B in NE-SW and for part C in NNE-SSW direction (Figure 3.23). However, it can be said that the extension direction is close to each other. The maximum stress ( $\sigma_1$ ) is almost vertical for all parts at first location. The R-value for all parts is calculated as 0.50, and the stress regime of the fault at three locations is showing pure extension characteristic (Figure 3.4).

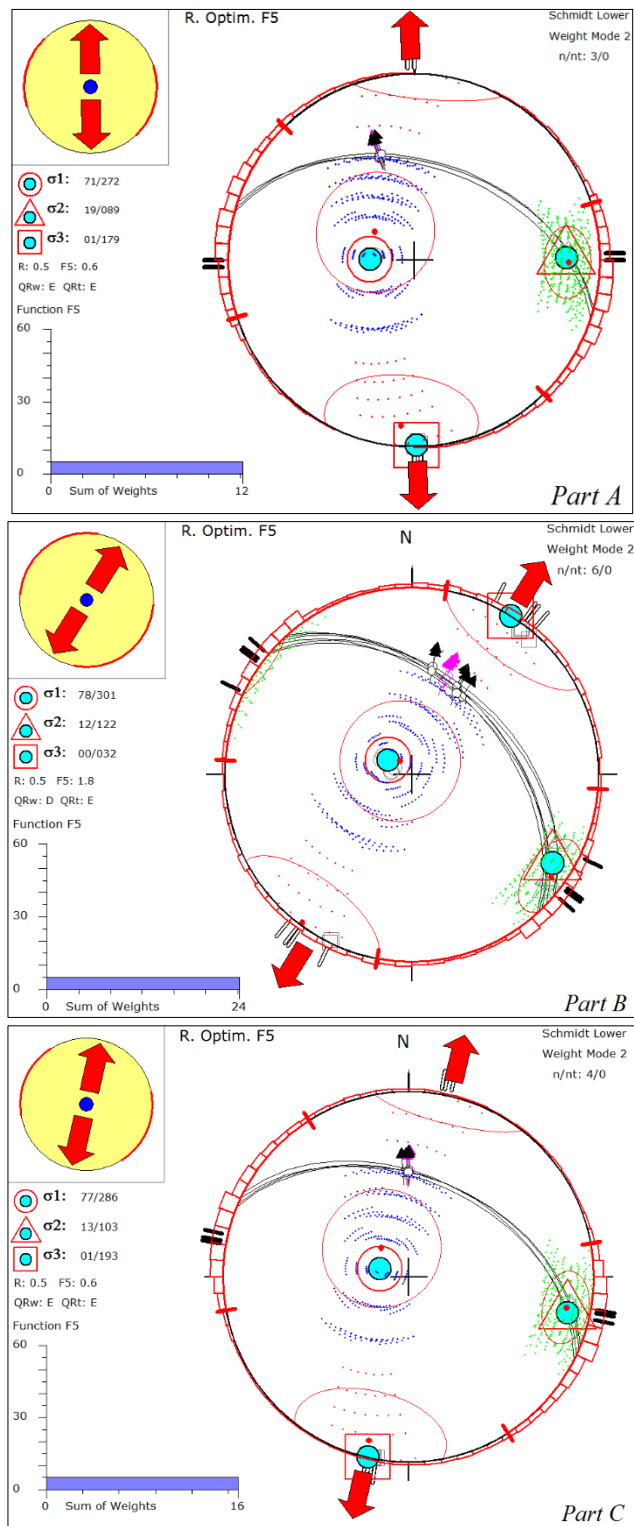


Figure 3.22. The principal stress axes of all parts along the Manisa Fault.

Sketch plan view of the fault plane evaluated at first location along the Manisa Fault (Figure 3.23). As it can see from the figure, the trend of the fault plane is turning between part A and part C. Solid black colored line represents the fault plane, and the south of the plan view is hanging wall block while the north is footwall block. This means that the fault plane is dipping to northeast, and the block is sliding towards north. The arrow lines represent the slickenlines observed on the fault plane. By dividing the fault plane into three parts, they are analyzed in terms of kinematic evolution. For all parts, the maximum compression is vertical, and their extension directions were obtained separately. The stress regime of the parts can be accepted as pure extension according to the ratio of principal stress differences and the fault is a normal fault (Figure 3.6).

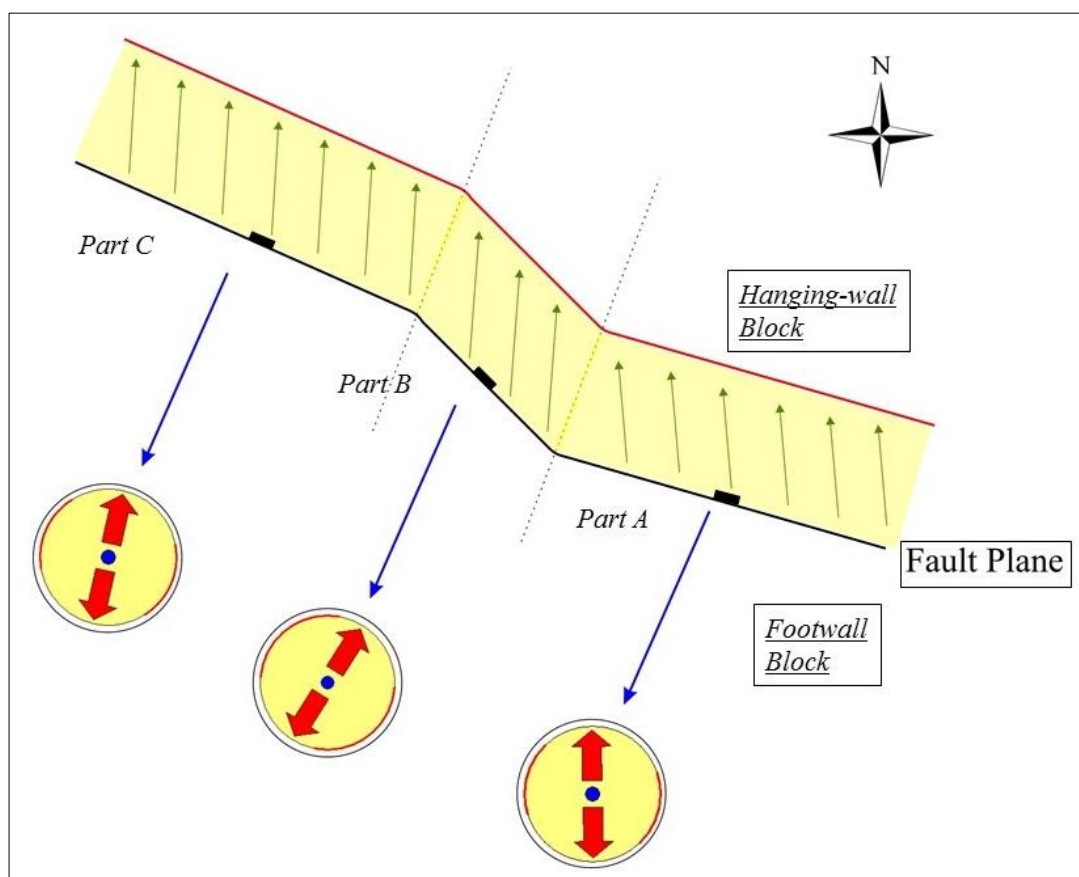
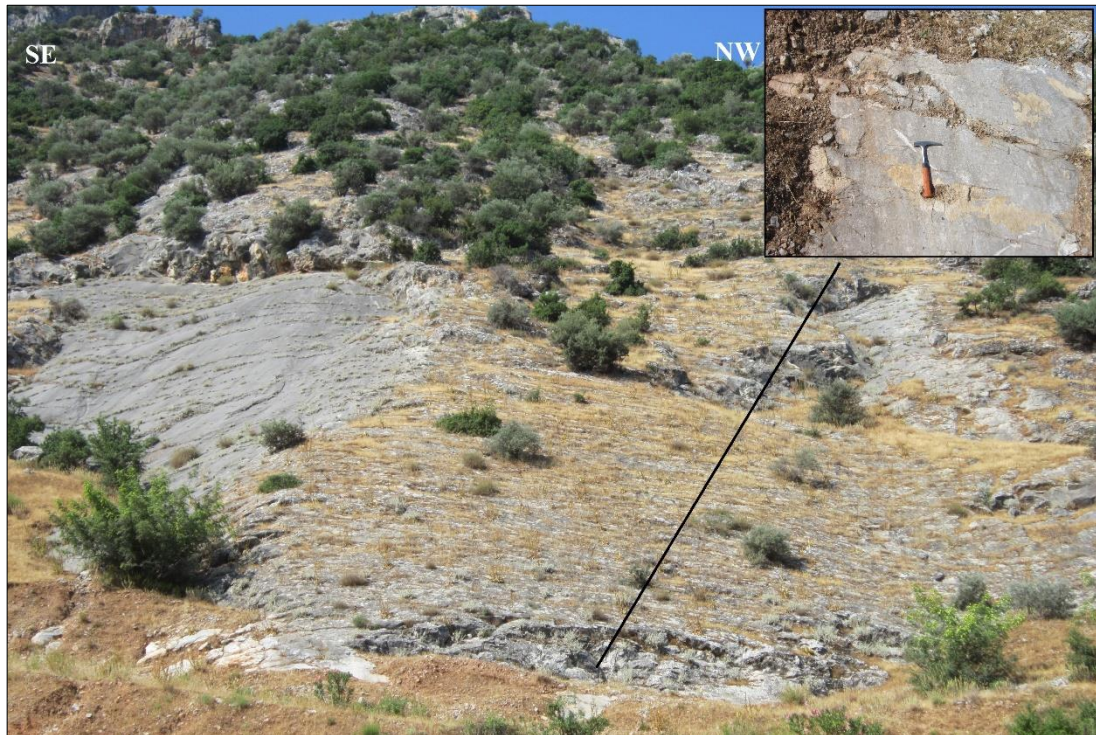


Figure 3.23. Sketch plan view of the fault plane observed at Location 01 along the Manisa Fault with stress symbols.

- Location 02 (Manisa Fault)

At Location 02, 9 slip-data were measured from the fault plane. The general trend of the fault plane is changing from 294°N to 310°N. The plane is dipping 37°, and 40° to northeast (Figure 3.24). The principal stress axes and the R-value were calculated for the kinematic analysis.  $\sigma_1$  (maximum stress) is 81/341,  $\sigma_2$  (intermediate stress) is 06/113, and  $\sigma_3$  (minimum stress) is 07/204 (Figure 3.25). The stereoplots of the principal stress axes show that the maximum compression is almost vertical. The fault obtained at second location has NE-SW extension. The R-value is 0.50. Therefore, the fault has pure extension characteristic (Figure 3.4), and the fault is a normal fault (Figure 3.5).



*Figure 3.24.* The fault plane evaluated at Location 02 has NW-SE trending with NE dipping (E: 545996, N: 4270827, Zone: 35).

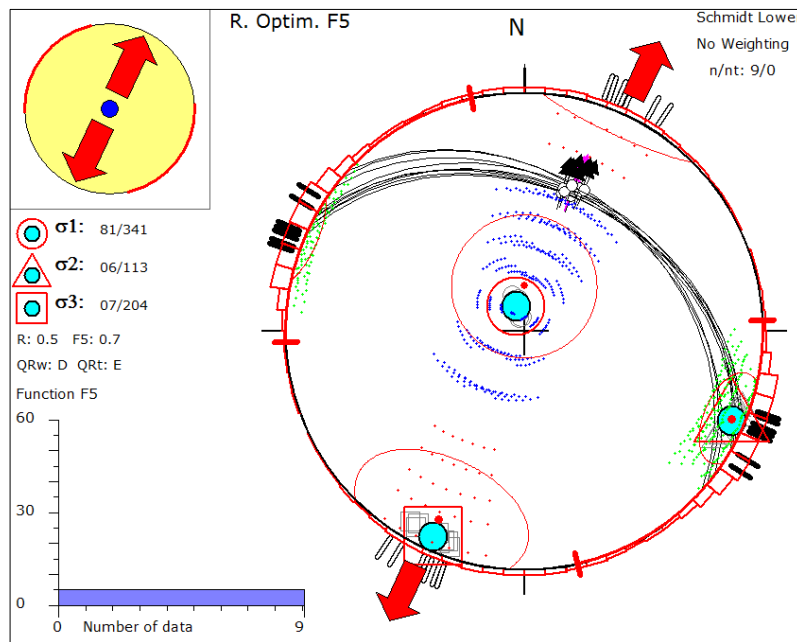


Figure 3.25. The principal stress axes of the fault plane examined at Location 02 along the Manisa Fault.

- Location 03 (Manisa Fault)

At Location 03, 26 slip-data were collected from the fault plane. The general trend of the fault plane is between  $310^\circ\text{N}$  and  $321^\circ\text{N}$ . The fault plane is dipping  $52^\circ$ - $59^\circ$  to northeast (Figure 3.26). By using collected measurements, the principal stress axes and the ratio of principal stress differences are calculated for the kinematic analysis. The stress orientations are  $\sigma_1$  (maximum stress) is 77/258,  $\sigma_2$  (intermediate stress) is 08/130, and  $\sigma_3$  (minimum stress) is 10/038 (Figure 3.27). According to these results, the maximum stress value is almost vertical, and the fault resulted from NE-SW extension. The R-value is determined as 0.50. The stress regime is pure extension according to the R-value (Figure 3.4), and the fault is a normal fault (Figure 3.5).

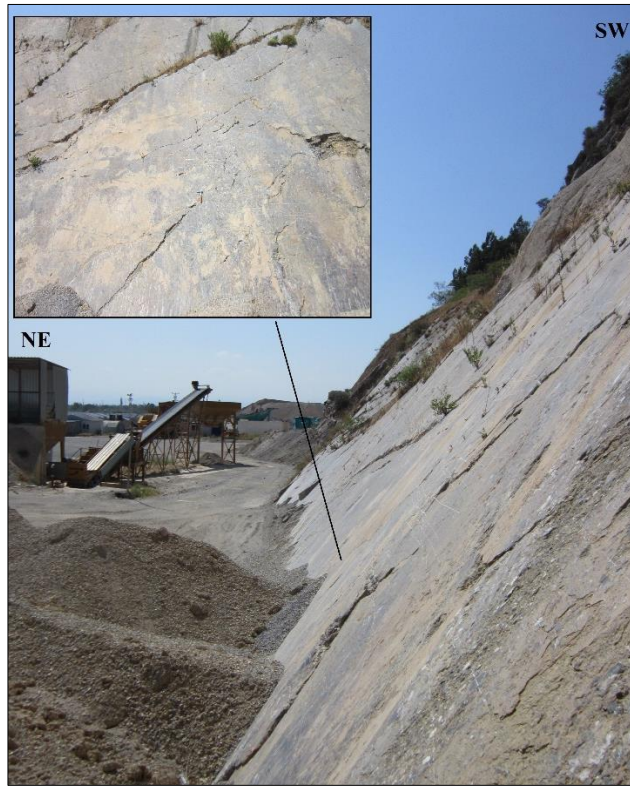


Figure 3.26. The fault plane evaluated at Location 03 has NW-SE trending with NE dipping (E: 546883, N: 4270145, Zone: 35).

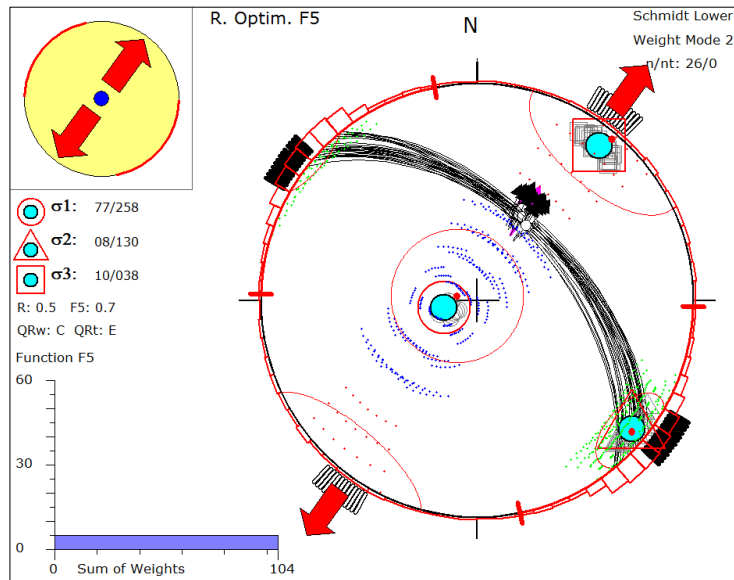


Figure 3.27. The principal stress axes of the fault plane examined at Location 03.

The slip-data were collected from 7 locations with 12 resolutions within the study area to analyze the kinematic evolution (Figure 3.28). Only at two locations, where the trend of fault plane is changing, the principal axes and the R-value were determined separately to obtain better results. As it can be understood from the kinematic map (Figure 3.28), all faults examined in the field have same characteristics in terms of stress regime because of having same the R-value. The ratio was defined as 0.50 for all of them, and the stress regime for all analysis shows pure extension characteristics, and all evaluated faults are normal faults.

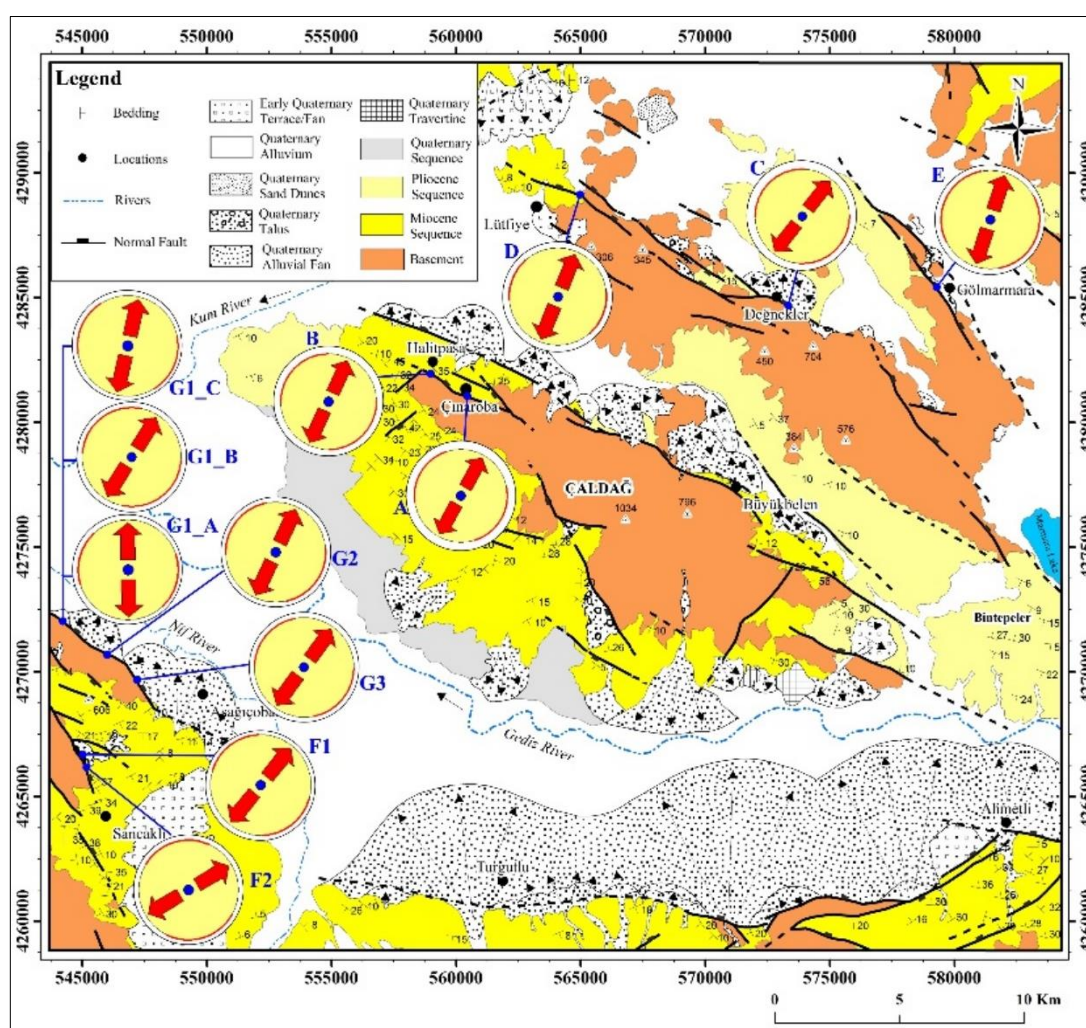


Figure 3.28. The kinematic map with stress symbols. A: Çınaroba Fault, B: Halitpaşa Fault, C: Değnekler Fault, D: Lütfiye Fault, E: Gölarmara Fault; F1 & F2: The faults evaluated in Sancaklıkayadibi, G1, G2 & G3: the Manisa Fault evaluated at three locations.

### 3.3.8. The Akhisar Fault (Karahöyük Mountain)

Karahöyük Mountain is located approximately at 4.5 km south of Akhisar city. Along north and south sides of the mountain, the Akhisar fault can be observed with huge fault planes (Figure 3.29). The fault at north is named as the North Akhisar Fault, and the fault at south is named as the South Akhisar Fault. Although the area is being outside of the study area, the region is a part of the GAG in terms of tectonic evolution. 44 slip-data were collected from the fault plane, and according to these data, it is said that the North Akhisar Fault and the South Akhisar Fault have the same general trend in NW-SE direction, but the faults are dipping to opposite directions. While the North Akhisar Fault is dipping to northeast, the South Akhisar Fault is dipping to S-SE direction. In following, these issues will be explained. The Karahöyük Mountain is a horst between these faults. The lithological unit dominating the Karahöyük Mountain Horst is generally marble and the fault measurement were taken from the fault planes formed in this unit (Figure 3.29 & Figure 3.30).

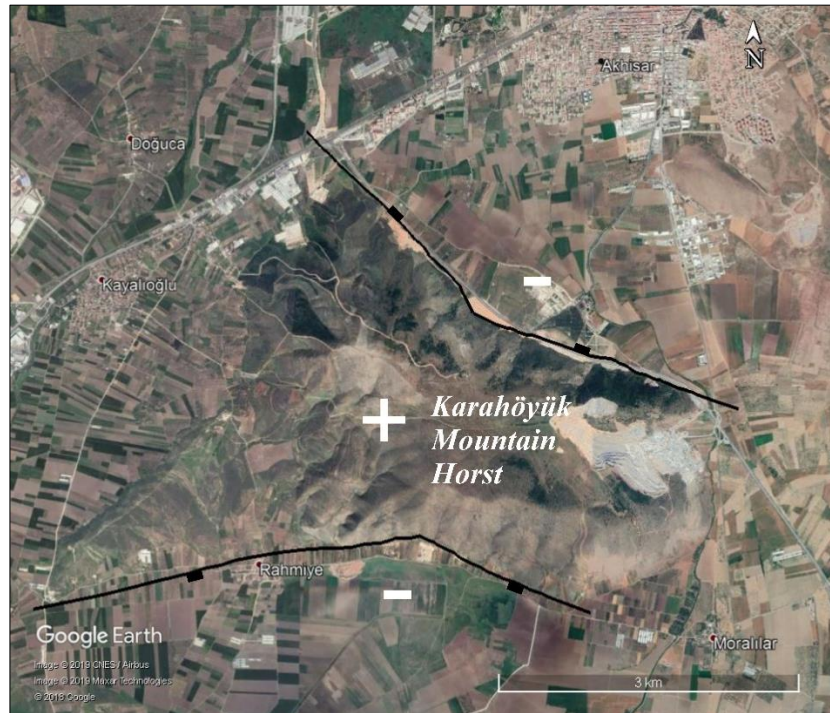


Figure 3.29. The location map of the Karahöyük Mountain Horst at south of Akhisar.

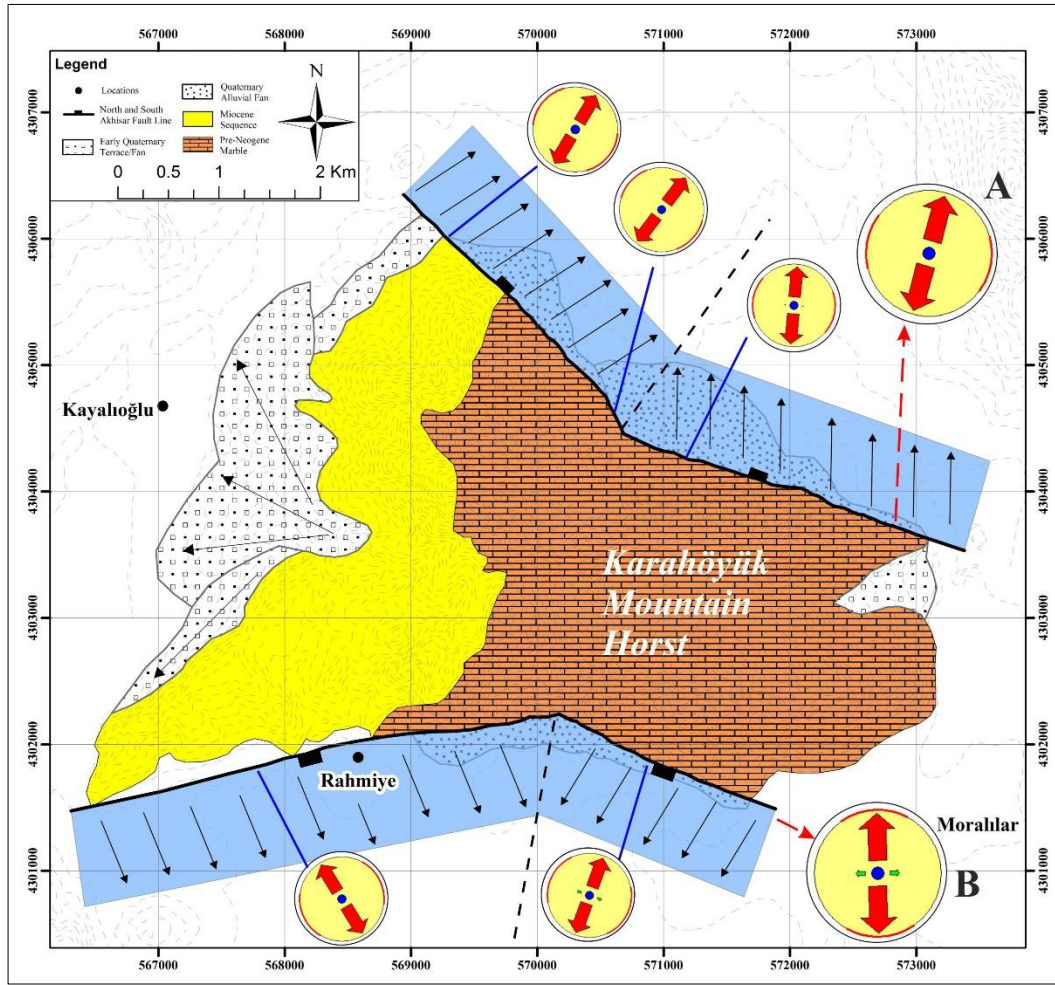


Figure 3.30. The map showing stress regime symbols of north and south Akhisar Fault with lithological units.

- North Akhisar Fault

31 slip-data were collected from totally 7 fault planes along the northern slope of the Karahöyük Mountain Horst. According to the measurements from the fault planes, it is seen that there are three trends for North Akhisar Fault. That's why the fault was divided into three parts according to the fault trend. These trends are  $312^{\circ}\text{N}-319^{\circ}\text{N}$ ,  $325^{\circ}\text{N}-339^{\circ}\text{N}$ , and  $290^{\circ}\text{N}-305^{\circ}\text{N}$  respectively from northwest to southeast. North Akhisar Fault is dipping  $45^{\circ}-70^{\circ}$  to northeast (Figure 3.30). The principal stress axes and the ratio of principal stress differences were calculated for parts separately along the northern slope of the mountain (Table 3.2).

Table 3.2. *The principal stress axes and the ratio of principal stress differences results for the North Akhisar Fault.*

Part	$\sigma_1$		$\sigma_2$		$\sigma_3$		R
	Trend	Plunge	Trend	Plunge	Trend	Plunge	
01	291	74	123	16	32	16	0.50
02	286	57	142	28	43	16	0.50
03	254	68	101	19	8	9	0.48

It can be understood from the stereoplots of the principal stress axes, the maximum stress value is almost vertical for all parts. While the first and second parts have an extension in NE-SW direction, the extension of part 03 is in NNE-SSW direction (Figure 3.31). The R-value is 0.50 for the first and second part, and the ratio of part 03 is 0.48. As it is understood from the table of the meaning of stress regime, the North Akhisar Fault has pure extension characteristic (Figure 3.4), and the fault is a normal fault (Figure 3.5).

- South Akhisar Fault

13 slip-data were collected from totally 3 fault planes along the southern slope of the Karahöyük Mountain Horst. According to the measurements from the fault planes, it is seen that there are two trends for South Akhisar Fault. That's why the fault was divided into two parts according to the fault trend. These trends are 79°N-85°N, and 110°N-135°N respectively from west to east. The dip directions of two parts differ from each other, While the first part is dipping 52°-67° to southeast, the second part is dipping 35°-57° to northwest (Figure 3.30). The principal stress axes and the ratio of principal stress differences were calculated for parts separately along the southern slope of the mountain (Table 3.3).

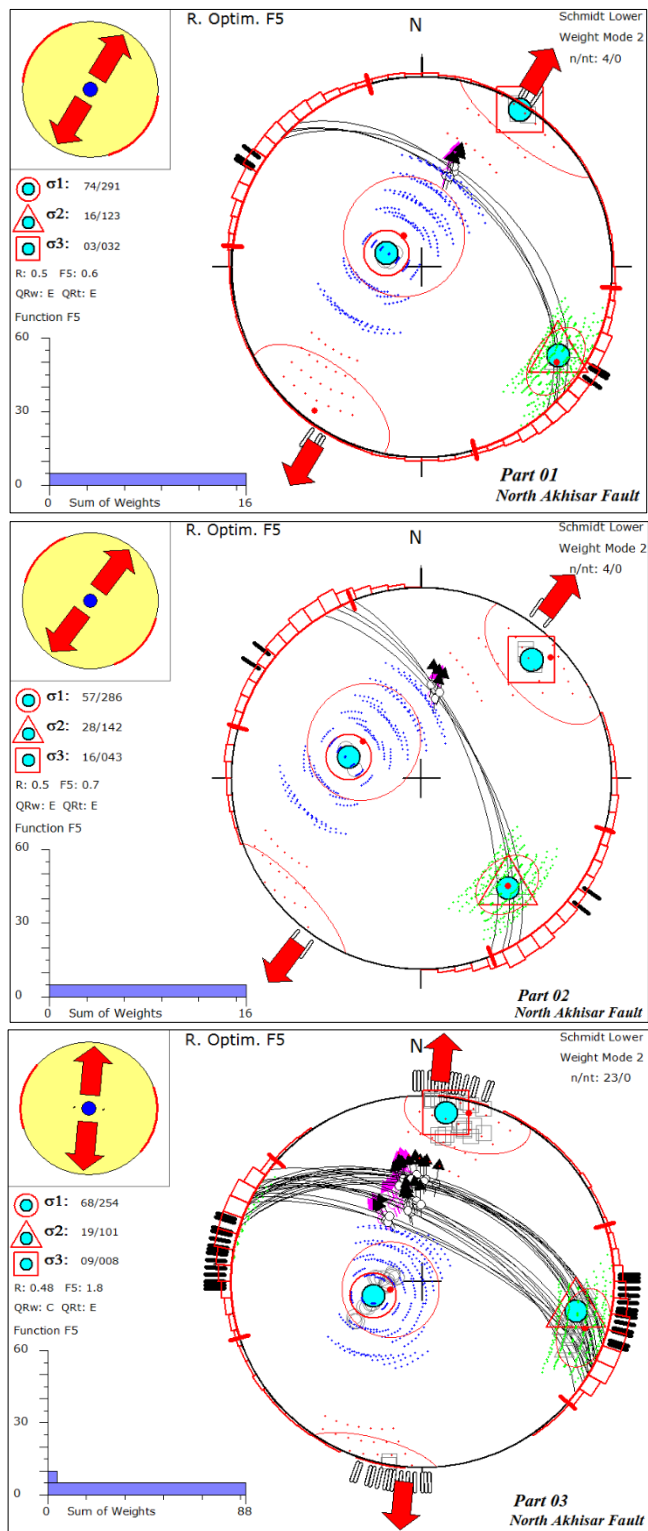


Figure 3.31. The principal stress axes of all parts along the North Akhisar Fault.

Table 3.3. *The principal stress axes and the ratio of principal stress differences results for the South Akhisar Fault.*

Part	$\sigma_1$		$\sigma_2$		$\sigma_3$		R
	Trend	Plunge	Trend	Plunge	Trend	Plunge	
1	25	69	246	16	153	13	0.50
2	127	75	287	14	18	5	0.43

It can be understood from the stereoplots of the principal stress axes, the maximum stress value is almost vertical for all parts. While the first part has an extension in NW-SE direction, the extension of second part is in NE-SW direction (Figure 3.32). This means that South Akhisar Fault trend is turning at the center. The R-values are 0.50 and 0.43 respectively. As it can be understood from the table of the meaning of stress regime, the fault at first part has pure extension characteristic in terms of stress regime, but for the second part, the stress regime is pure to radial extension (Figure 3.4), and the fault is a normal fault (Figure 3.5).

The North Akhisar Fault is divided into three parts in terms of fault elongation while The South Akhisar Fault is divided into two parts. At the beginning, the faults were evaluated kinematically without separating into parts in terms of their strikes. Stress regimes acting on North and South Akhisar Fault (A & B) indicate i) for the North Akhisar Fault, there is an extension in NNE-SSW direction, ii) for the South Akhisar Fault the extension is in N-S direction (Figure 3.30). This situation was different when the faults were evaluated by separating into parts based on the strikes of faults. In the first 2 parts of the North Akhisar Fault, there is a NE-SW extension, and in the third part, the extension in NNE-SSW direction was evaluated (Figure 3.30). Similar situation is observed in the South Akhisar Fault. For the first part, the extension is in NW-SE direction, while for the second part it is in NE-SW direction (Figure 3.30).

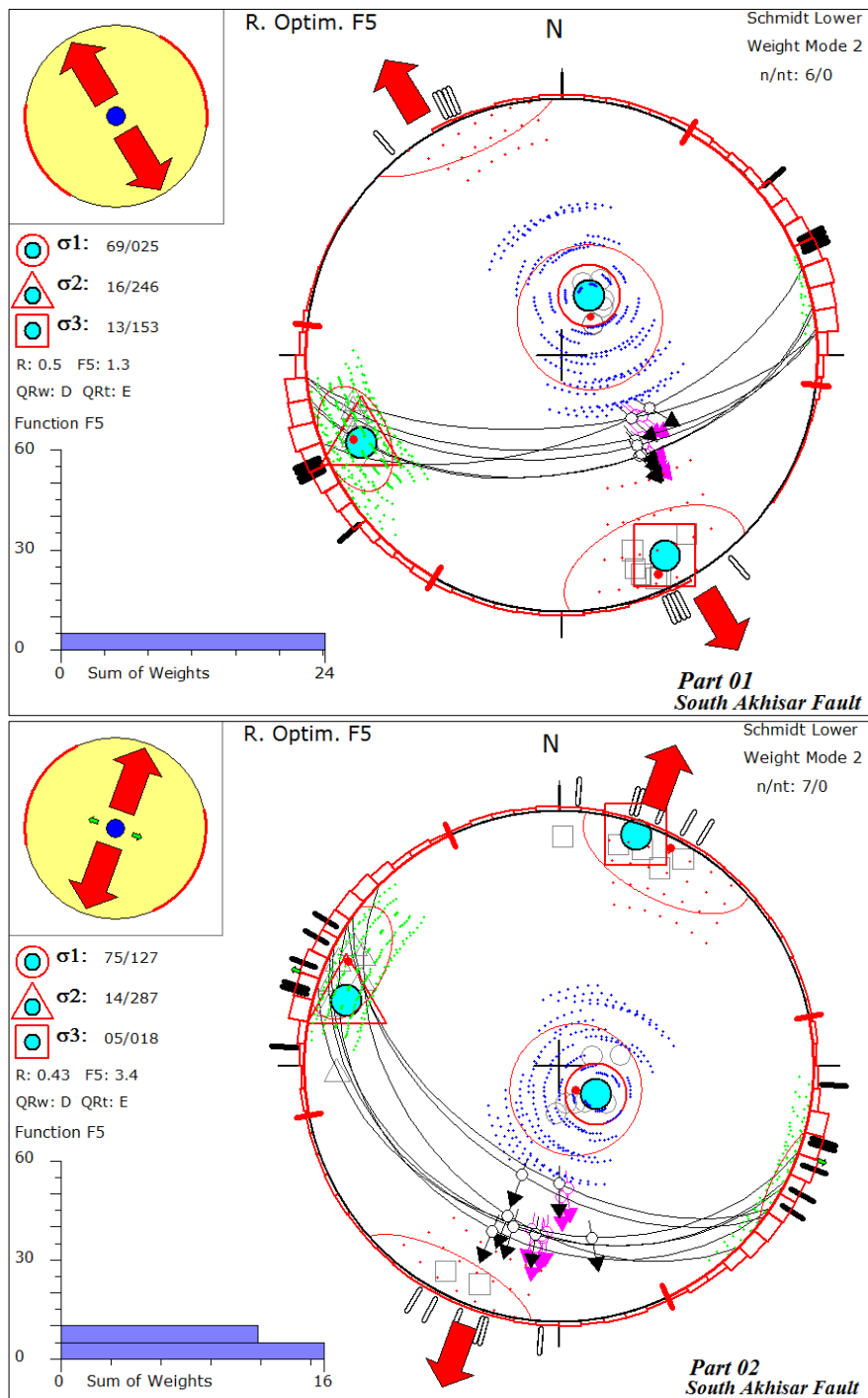


Figure 3.32. The principal stress axes of all parts along the South Akhisar Fault.

## CHAPTER 4

### MORPHOMETRIC ANALYSIS

Morphometry is the measurement of landscape shape quantitatively (Keller and Pinter, 2002). This measurement helps to compare different landforms by using geomorphic indices that are useful tools to identify the tectonic activity. There are some geomorphic indices for tectonic activity. The indices that are used in this study are the asymmetry along the ridges and the mountain front sinuosity (Smf).

#### 4.1. Asymmetry along the Ridges

This method is evaluated into two main parts which are the slope analysis, and the asymmetry ratio of the ridges.

The slope analysis were conducted for three mountain ridges defined as Çaldağ, Değnekler and Gölarmara for this study. The reason for the slope analysis is to understand the surface slope changes depending on elevation movements. Firstly, slope analysis view was obtained by DEM created for the study area by using *ArcGIS 10.4.1* software. This view is created in two ways. While the first way is created according to the slope changes in degree (Figure 4.1), the second one is created according to the slope changes in percentage for the study area. There is an important situation to consider at this point. While the software program creates these two slope maps, the slopes within the stream channels was considered with the surface slope. This leads to infollution to evaluate the slopes of the regions and does not proper for our purpose. Figure 4.2 explains what we consider for slope analysis. Blue colored arrows show the stream channel slope in the region, and red colored arrows represent the surface slope. In this context, the surface slope of the ridges was considered for this study.

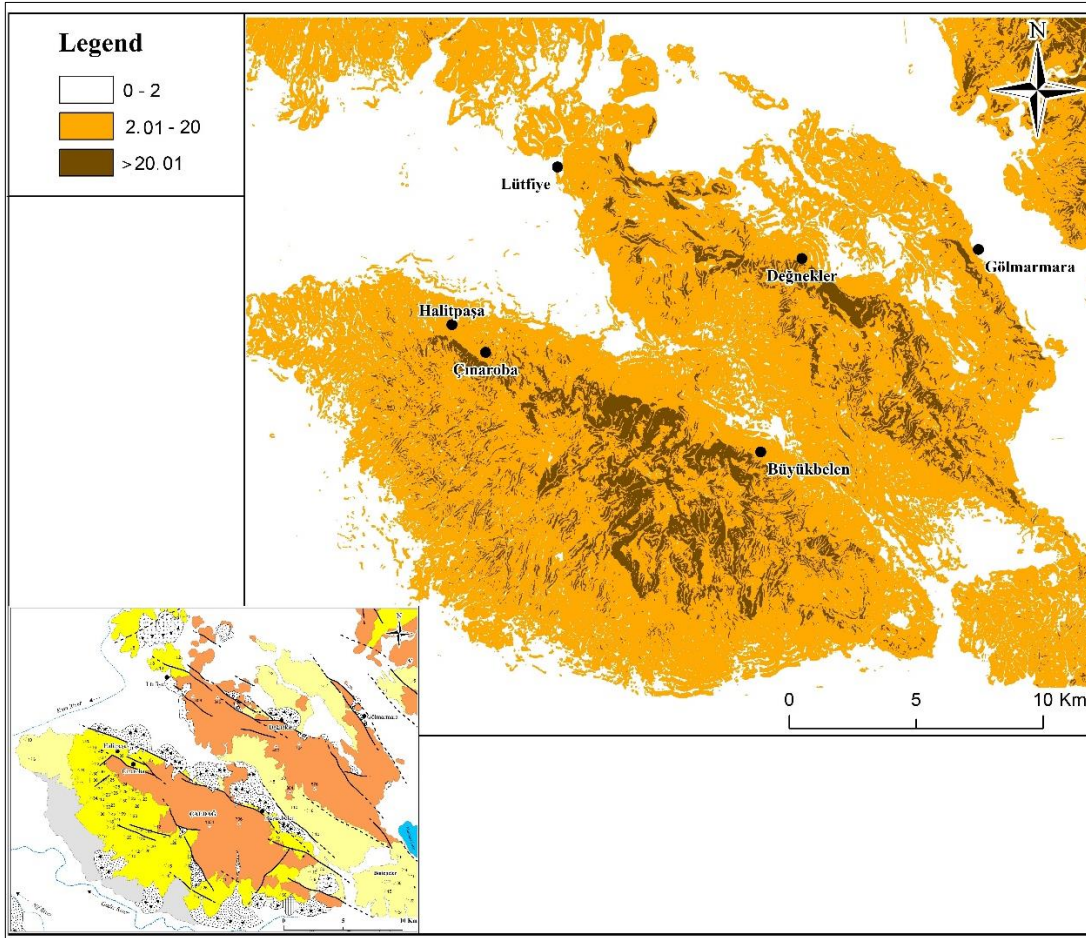
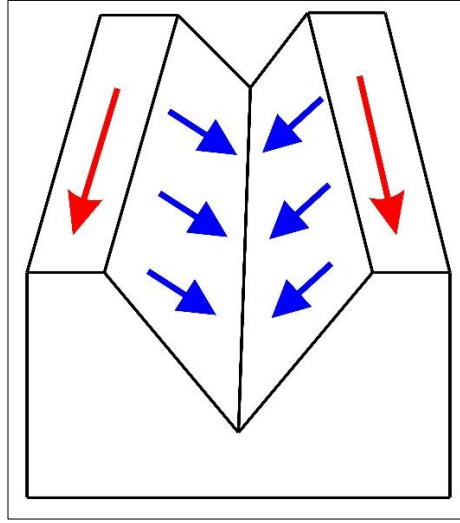


Figure 4.1. Slope map view showing degree changes in the region (Please see Figure 2.1 for the legend of generalized geological map).

In this study, in order to evaluate the surface slope analysis, another method was defined apart from the slope maps obtained from the software. This method can be defined as the correlation of the surface slope changes obtained at the profiles drawn throughout the mountainside. Firstly, the water divide lines were determined for all three ridges to draw the profile lines. While drawing the water divide lines, stream map obtained by ArcGIS software (Figure 4.3) and topographic maps were used. The water divide line can be assumed as the division line of the mountain and it indicates where the streams flow along the mountainside.



*Figure 4.2.* Sketch draw showing surface slope in red colored arrows and stream channel slope in blue colored arrows.

Totally 34 profile lines were drawn for three ridges in SW-NE direction (Figure 4.4). 14 profiles out of 34 were determined for Çaldağ Ridge while 12 profiles out of 34 were determined for Değnekler Ridge. Remaining 8 profiles were drawn for Gölarmara Ridge. The profile lines drawn for each mountain are combined in the water divide line and the continuity of each other is ensured. Thus, the surface slope change was determined on both sides of the mountains. In order to classify each slope changes, the slope range scale was determined. Table 4.1 shows this determined scale with determined colors. Also, the defined lithological units were shown by using letters at all of 34 profiles and Table 4.2 shows the lithological units with used letters.

The surface slope change can depend on many factors in the region. The change in surface slope may be affected by lithological diversity. As the resistance of each rock to erosion in nature will be different, slope changes can be seen on the surface due to erosion. Also, the slope changes can be observed in the profiles depending on the fault planes detected in the study area. All of 34 profiles are examined in detail for each ridge in terms of lithology and fault.

Table 4.1. The range of slope change with color legend for slope modeling.

Slope Range Scale	Color Legend
$0^\circ \leq \text{Slope} \leq 2^\circ$	Red
$2^\circ < \text{Slope} \leq 20^\circ$	Yellow
$\text{Slope} > 20^\circ$	Orange

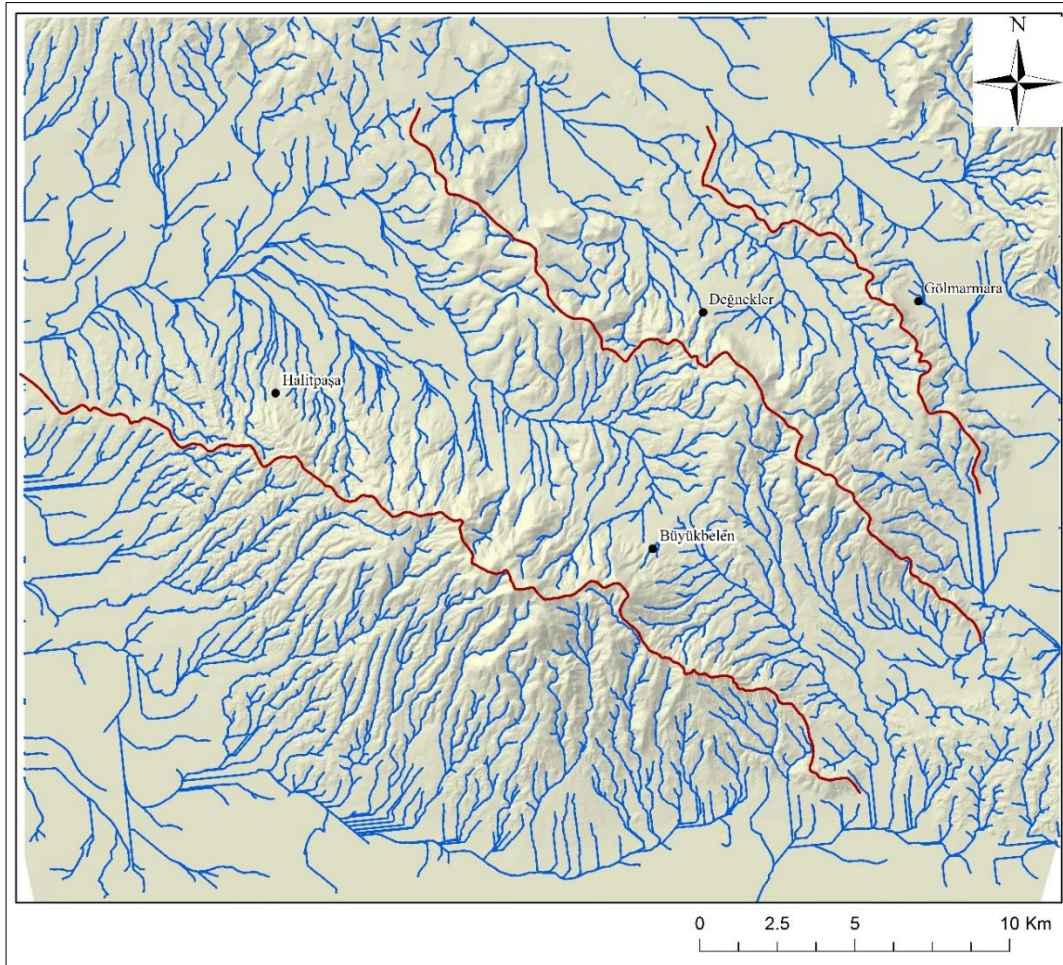


Figure 4.3. Water divide lines belonging to three ridges with streams obtained from ArcGIS 10.4.1 software.

Table 4.2. Lithological units with defined letters for cross sections.

Lithology	Letter
Basement	A
Miocene Sequence	B
Pliocene Sequence	C
Quaternary Sequence	D
Quaternary Travertine	E
Quaternary Alluvial Fan	F
Quaternary Talus	G
Quaternary Alluvium	H
Early Quaternary Terrace/Fan	J

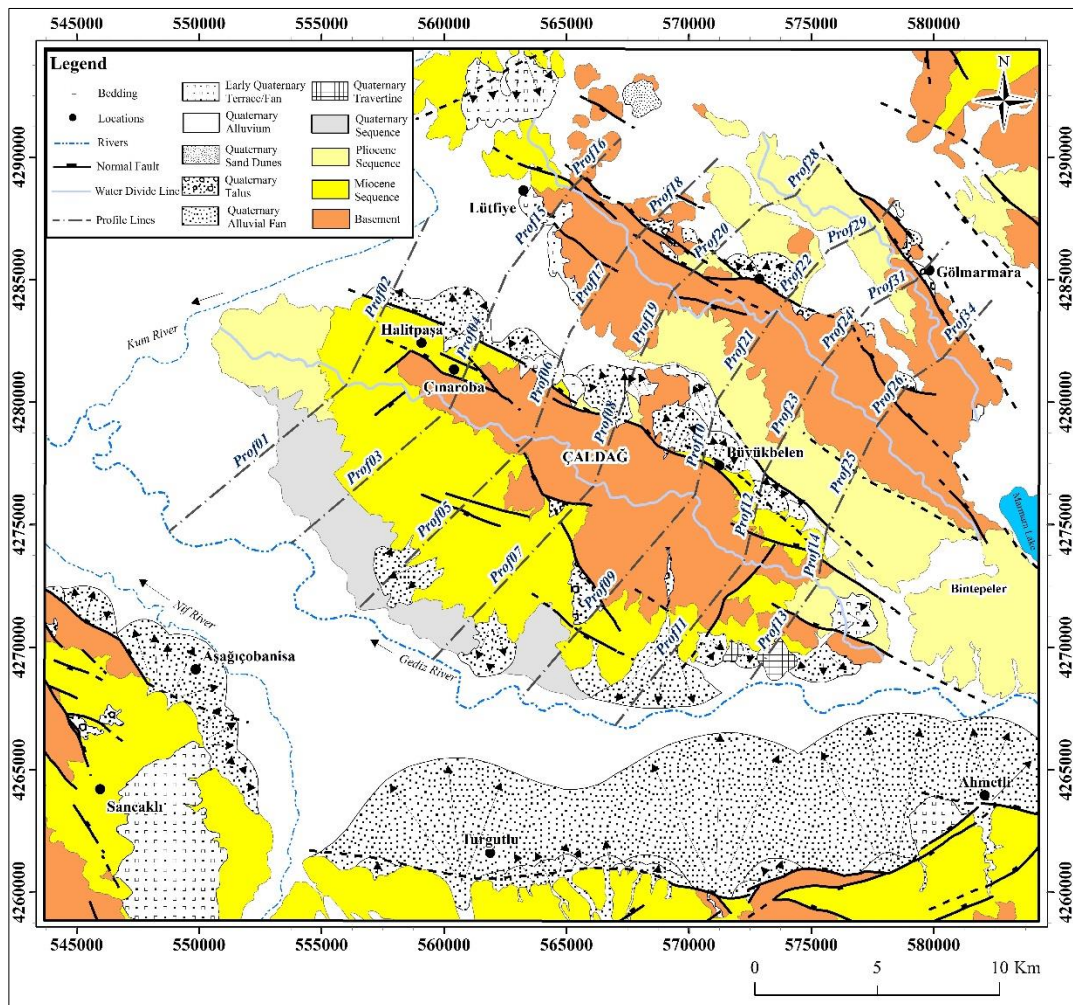


Figure 4.4. The geology map showing profile lines for three ridges.

#### 4.1.1. The Çaldağ Ridge

14 profiles out of 34 were drawn for the Çaldağ Ridge (Figure 4.5). The lineation of these profiles is SW-NE direction. Half of the profiles are located at the southwest side of the mountain and the remaining are located at the northeast side. Water divide line can be assumed as an imaginary line for all 14 profiles (Figure 4.4). The slope changes were evaluated for both sides of the mountain from the ground level to the top of the mountain. Thus, the positive sign implies the slope increase whereas the negative sign implies the slope decrease. The lithological units and faults defined on the geological map were shown at all profiles.

*Profile 01;* The topography is continuing gently in this profile.

*Profile 02;* The slope increase was determined at the middle of the profile and this increase may mean the existence of the fault defined as the solid line in the geological map.

*Profile 03;* The slope increase was determined at the top of the mountain and this may be directly related with the basement. Due to the resistance to the erosion, this slope increase may be formed.

*Profile 04;* The slope increases show the existence of the faults in the region. The fault defined as the solid line at the right side of the section is same with the fault determined at Profile 02. These are having the same characteristics. Also, the fault which is located at the left side of the section is evidence of the fault observed at the region.

*Profile 05;* There is an increasing inclination towards the summit. The first fault defined as the solid line at the left side of the profile shows the existence of the fault in the region. Also, at the top of the mountain, it can be clearly seen that there is a sudden increase in the slope, and this means the fault defined as the dashed line is exist in the region.

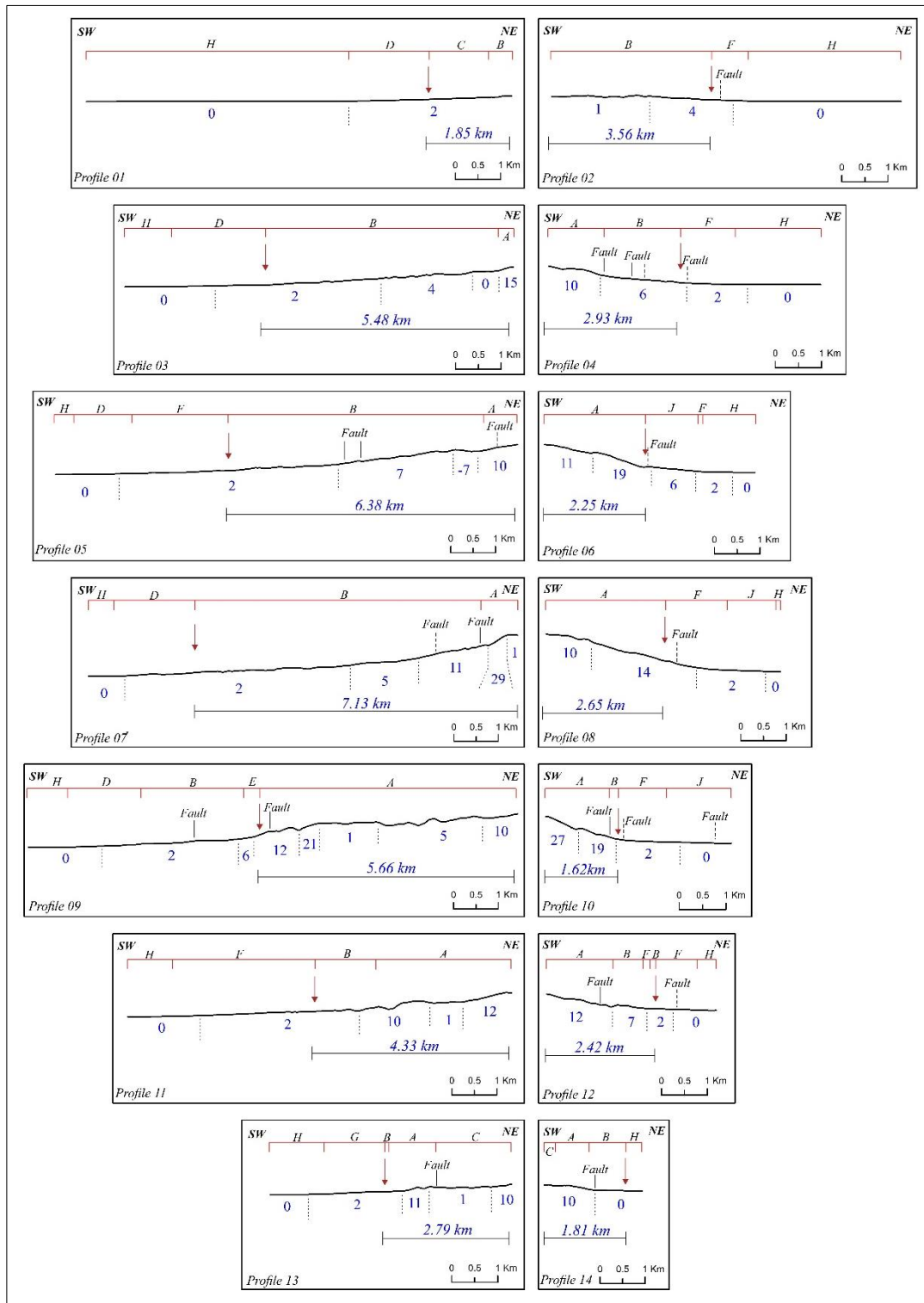


Figure 4.5. 14 profiles drawn for the Çaldağ Ridge showing slope changes and the width of the profiles.

*Profile 06*; The slope is increasing from the middle of the profile to the summit, and the fault defined as the dashed line is the clue of the existence of the fault, and it is the continuity of the fault observed in Profile 02 and 04. They have the same characteristics.

*Profile 07*; The slope is increasing towards the summit and it can be said that both the faults defined at profile exist in the region and especially second fault drawn as the solid line shows its effect clearly. The slope increased gently within the basement unit.

*Profile 08*; The slope is changing gently from the ground level to the top of the mountain for this profile. The fault defined as the dashed line shows the existence at the region.

*Profile 09*; The slope is increasing gently until the middle of the profile and after that point the slope shows sudden decreases. Especially the slope defined as 5° in the profile has a wavy appearance. The reason for this can be related with the erosion.

*Profile 10*; The slope is increasing sharply from the middle to the top of the mountain, and this is related with the determined two faults in the region. The slope change shows the direct relation with the fault existence.

*Profile 12*; It can be understood from the profile that the fault drawn as the solid line shows the existence in the region. Sudden slope increase was determined within the basement.

*Profile 13*; There is gently slope increase until the middle of the profile and the fault shown its own characteristic defined in the field.

*Profile 14*; There is sudden slope increase and before the increase, the fault with the solid line was determined. This fault has the continuity of the fault observed in Profile 12.

#### **4.1.2. The Değnekler Ridge**

12 profiles out of 34 were drawn for the Değnekler Ridge (Figure 4.6). The lination of these profiles is SW-NE direction. Half of the profiles are located at the southwest side of the mountain and the remaining are located at the northeast side. Water divide line can be assumed as an imaginary line for all profiles (Figure 4.4). The slope changes were evaluated for both sides of the mountain to the top. Thus, the positive sign implies the slope increase whereas the negative sign implies the slope decrease at all profiles. The lithological units and faults defined on the geological map were shown at all profiles.

*Profile 15;* After the wide flatness, the slope is increasing, and the reason of this increment can be the fault observed at the region. Towards the summit, because of the basement, the slope is increasing.

*Profile 16;* The faults observed at the region with normal characteristics were observed at this profile. These faults are defined as normal faults dipping to the northeast at Figure 4.4. As can be seen from the profile, a decrease in topography towards the northeast is observed.

*Profile 17;* Until the middle of the profile, the slope is increasing. As can be seen from the profile, because of the fault defined as the dashed line, the increment of the slope can be explained.

*Profile 18;* After the wide flatness, the slope is increasing suddenly. The reason for this increment can be the lithological unit which is the basement and the fault defined within the wide flatness region. Towards the top of the mountain, the slope is increasing again. There are two faults drawn in the profile, and the reason for the increment can be these faults. Moreover, the slope changes were observed at the basement.

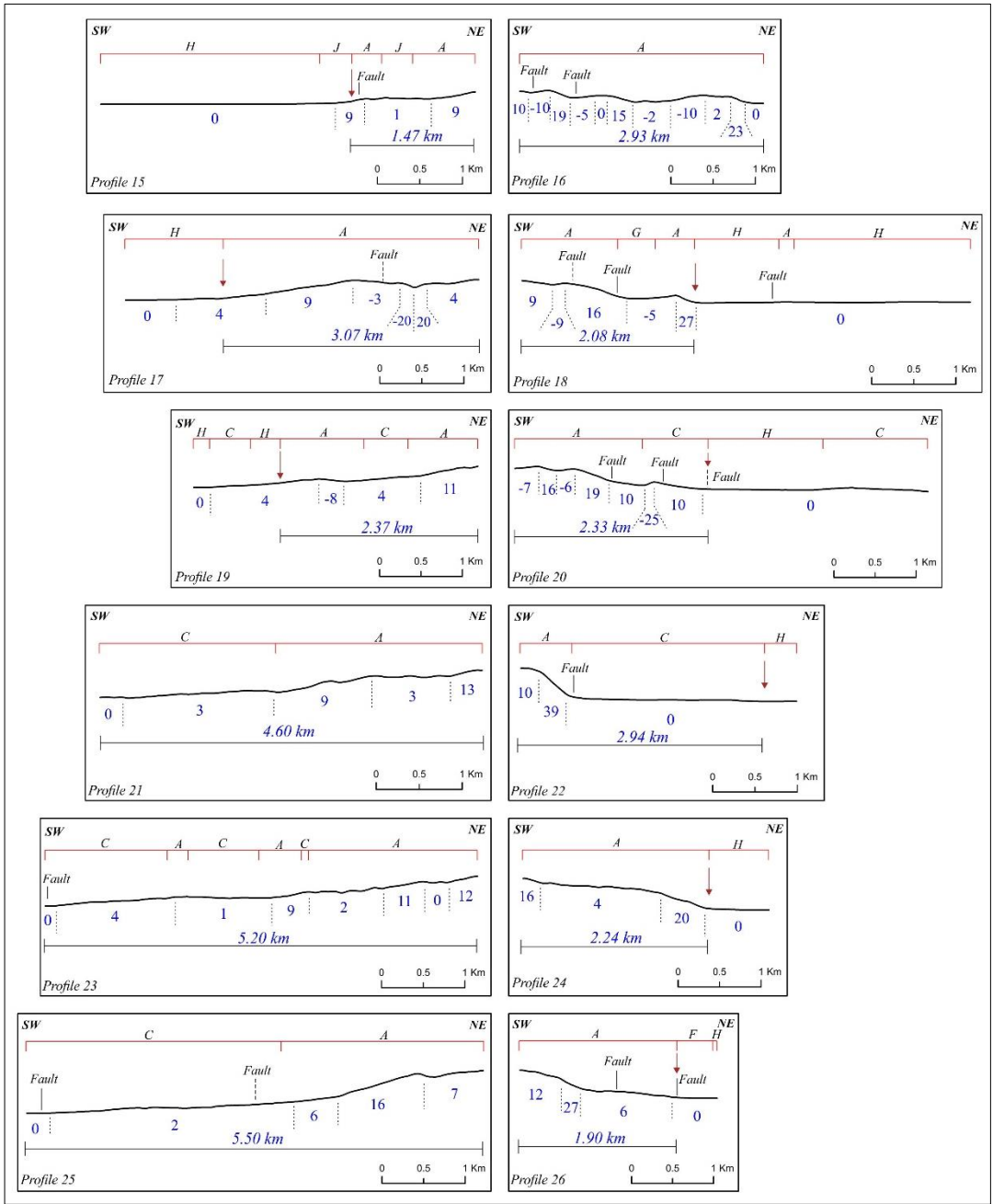


Figure 4.6. 12 profiles drawn for the Değnekler Ridge showing slope changes and the width of the profiles.

Profile 19; At this profile, there are not any faults defined at the region. However, the slope is generally increasing from ground level to the top of the mountain. The reason for the slope change can be erosion at the region.

*Profile 20;* After the wide flatness, the slope is increasing and after this increment, the slope is suddenly decreasing. These can be explained by the faults observed at the region. The second fault have normal characteristic and its dip direction can be assumed as southwest. After this decrease, the topography is increasing again towards the top of the mountain, and the effect of another fault can be seen again. It can be understood that these faults show the evidence of existence in the region.

*Profile 21;* The slope is increasing towards the top of the mountain. After only 9 degrees of slope, there is a decrease in slope.

*Profile 22;* The fault drawn as the solid line in the profile shows the evidence of existence in the region because of the sharp slope change. As can be seen at Figure 4.6, the slope amount is  $39^\circ$ , this can be defined as the fault plane.

*Profile 23;* The slope of the profile shows differences at some locations because at some location while the slope is increasing, at another point the slope is decreasing. As can be seen at the profile and the geological map, there is not any defined fault, but this increment can be explained by some undefined and covered fault planes at the region. Also, the erosion factor can be another reason for this slope change.

*Profile 24;* The slope change was observed within the basement at this profile. There is not any defined fault, however, it can be assumed that this increment can be resulted from the fault which is not discovered and determined.

*Profile 25;* After a continuously increasing slope, the slope towards the top of the mountain ridges decreases. The lithological unit where the slope increases are clearly seen is the basement. Moreover, we can also talk about the effect of the fault drawn with a dashed line. This is a clue to the existence of the fault in reality.

*Profile 26;* The increase in slope is clearly seen in the profile. The effect of normal faults observed in the field, especially the one closest to the peak, is observed. As can

be seen in the geology map, the fault is dipping to the northeast and this effect is clearly seen in the section.

#### **4.1.3. The Gölarmara Ridge**

8 profiles were drawn for the Gölarmara Ridge (Figure 4.7). The lineation of these profiles is SW-NE direction. Half of the profiles are located at the southwest side of the mountain and the remaining are located at the northeast side. Water divide line can be assumed as an imaginary line for all 8 profiles (Figure 4.4). The slope changes were evaluated for both sides of the mountain to the top. Thus, the positive sign implies the slope increase whereas the negative sign implies the slope decrease at all profiles. The lithological units and faults defined on the geological map have been shown at all profiles.

*Profile 27*; The topography has gentle slope view.

*Profile 28*; The topography has a wavy view within the Pliocene sequence. The reason for this view may be the erosion effect.

*Profile 29*; The slope is increasing gradually towards the top of the mountain, and this increment is observed within the Pliocene sequence unit.

*Profile 30*; The profile drawn in the northeast side of the mountain has two defined faults, and their effects can be seen on the topography clearly. At the right side of the profile, there is sharp slope change within the basement, and this shows the fault effect at that point.

*Profile 31*; The slope is increasing towards the top of the mountain. There is not any defined faults, but the slope change can be resulted from the fault existence.

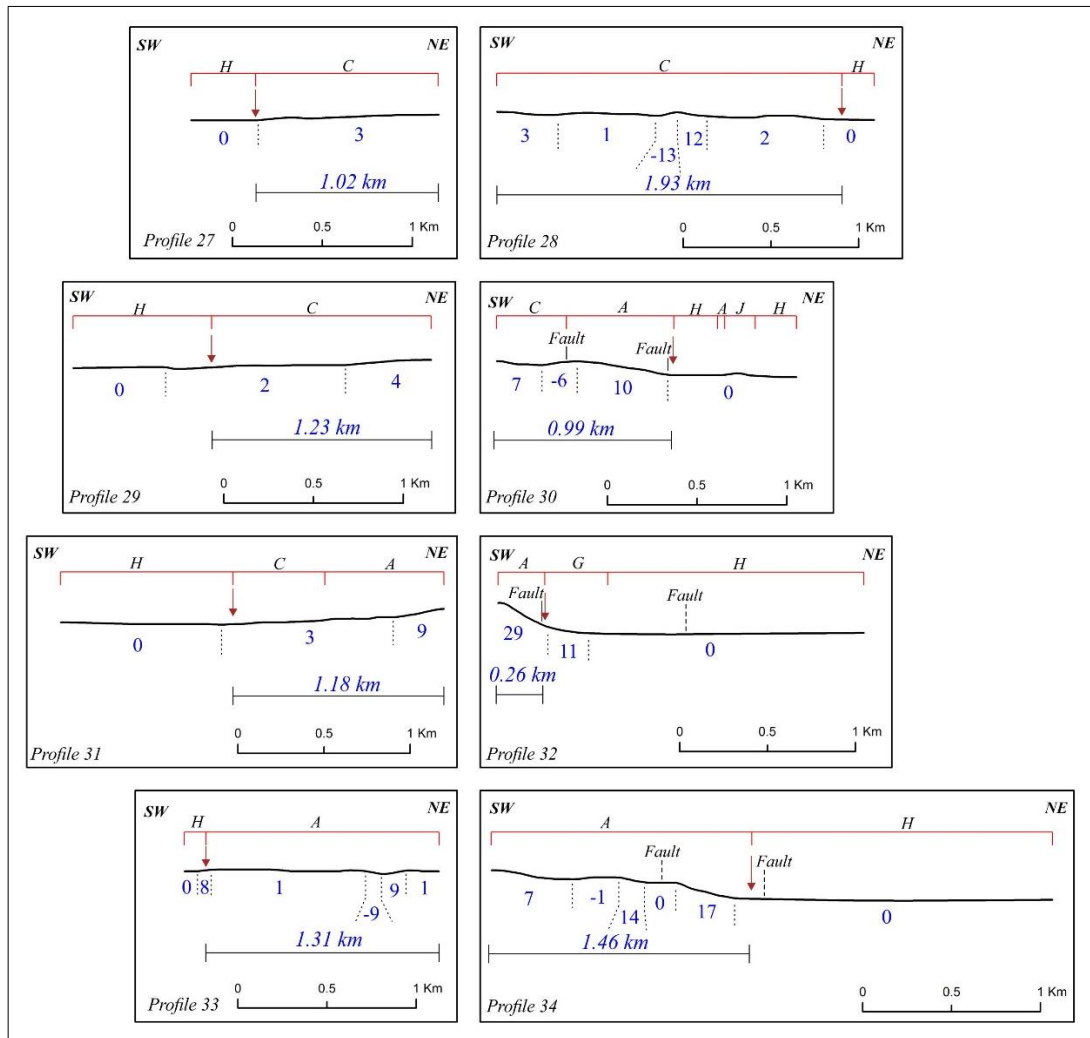


Figure 4.7. 8 profiles drawn for the Gölarmara Ridge showing slope changes and the width of the profiles.

*Profile 32*; The inclination is increasing towards the summit. The fault defined as the solid line in the cross section is the clue of the existence in the region because of the sharp slope change.

*Profile 33*; The slope changes are observed within the basement generally. The reason for these changes can be directly related with the erosion.

*Profile 34*; The slope of the topography is increasing from the middle of the profile to the top, and as it can be seen in the profile, after the faults defined as the dashed line the slope is increasing and these can be the clue of the existence of the faults.

34 profiles drawn to determine the slope changes in the ridges were used again to determine the asymmetry ratio. Basically, asymmetry is calculated according to the ratio of the width of the profiles on both sides of the mountain. The width of the profiles for three mountains has been determined separately (Figure 4.5, Figure 4.6, Figure 4.7). The formation of Quaternary sequences continues with Gediz River and alluvial fan effects within the study area. Thus, along the mountainside, the basement and Neogene sequences are continuously covered by the Quaternary deposits. This was considered when calculating the asymmetry ratio. The Quaternary units were ignored while asymmetry evaluation was performed in each profile. Lithologically end point of the Quaternary units are assumed as the Quaternary Knick Point at all profiles. This point was shown with brown colored arrow at all profiles, and the analysis has been conducted by considering this point. The line passing through the peak of the mountain is assumed as the centerline of the profiles, and the width of the profiles on both sides is determined according to the centerline and the Quaternary Knick Points. The ratio of width at both sides gives the asymmetry factor of the profiles. When the ratio is equal to 1, the profile is defined as a symmetric, but, if the ratio is greater or less than 1, the profile is defined as an asymmetric (Figure 4.8).

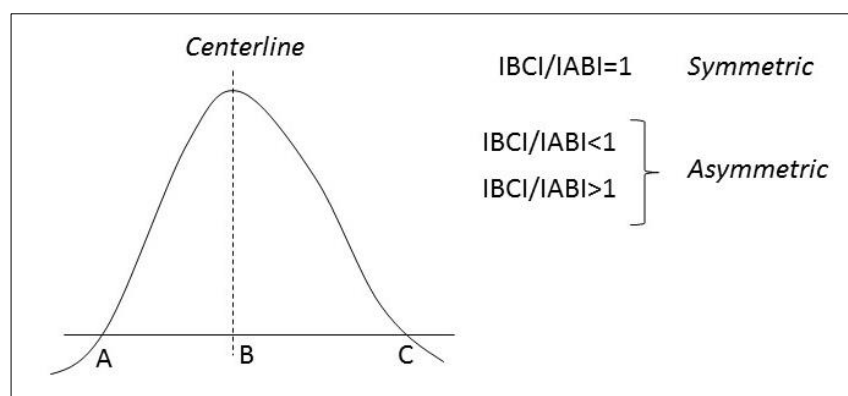


Figure 4.8. Determination of the asymmetry according to the width of the profile.

The asymmetry ratio of the profiles for three mountain ridges. It is possible to talk about asymmetry for three mountain ridges. The results are less than or greater than 1 and this is the sign of asymmetry (Table 4.3).

Table 4.3. *Asymmetry ratio results determined for each ridge.*

Asymmetry Ratio, Çaldağ		Asymmetry Ratio, Değnekler		Asymmetry Ratio, Gölmarmara	
<i>Prof01/Prof02</i>	1.93	<i>Prof15/Prof16</i>	1.98	<i>Prof27/Prof28</i>	1.89
<i>Prof03/Prof04</i>	0.53	<i>Prof17/Prof18</i>	0.68	<i>Prof29/Prof30</i>	0.81
<i>Prof05/Prof06</i>	0.35	<i>Prof19/Prof20</i>	0.98	<i>Prof31/Prof32</i>	0.22
<i>Prof07/Prof08</i>	0.37	<i>Prof21/Prof22</i>	0.64	<i>Prof33/Prof34</i>	1.12
<i>Prof09/Prof10</i>	0.29	<i>Prof23/Prof24</i>	0.43		
<i>Prof11/Prof12</i>	0.56	<i>Prof25/Prof26</i>	0.34		
<i>Prof13/Prof14</i>	0.65				

The results which are less or greater than 1 are the sign of the asymmetry of the ridges within the region. Generally, the width of the profiles located at the northeast of the ridges are shorter than the southwest profiles. According to this situation, it is said that the ridges are asymmetric, but there are some basic reasons for this asymmetry. Faulting and fault movements in the region are one of them. The effect of these faults is seen in many profiles. For all three mountain ridges, it is possible that the symmetry line shifts towards northeast due to the fault activity. When the profiles are evaluated lithologically, the slope changes are clearly defined. The slope change is mostly seen in the basement unit at all profiles. This is due to the erosion resistance of the rock type, and this proves the asymmetry of the mountain ridges in general.

#### **4.2. The Mountain Front Sinuosity (Smf)**

The Smf indicates the balance between erosional forces, tectonic forces, and fault activity. While erosional forces try to cut embayment as irregular and sinuous fronts, tectonic forces try to produce a straight mountain fronts (Bull, 1977; Bull and McFadden, 1977; Keller & Pinter, 2002). Mountain front sinuosity is defined by Bull (1977) as follows:

$$Smf = Lmf/Ls$$

$Smf$  is the mountain front sinuosity;  $Lmf$  is the length of the mountain front along the foot of the mountain, and  $Ls$  is the straight length of the mountain front (Figure 4.9). The mountain front is more sinuous with the vertical tectonic activity rate. Therefore, mountain fronts associated with active tectonics and uplift are showing straight formation. By contrast, when the uplift rate is decreased or ceases, erosion processes produce more irregular mountain front having high  $Smf$  value (Keller & Pinter, 2002; Azor et al., 2002). Disruption of faulting and decrease in activity lead to irregular mountain front with increasing  $Smf$  value. However, lower  $Smf$  values are obtained at greater uplift rates and resistant rock units. The  $Smf$  value which is less than 1.40 indicates generally active faulting (Bull & McFadden, 1977). There are two important point affecting  $Smf$  index results. These are resistance of rock unit and high sedimentation rate. If the rock unit is eroded easily, this will lead to obtain higher  $Smf$  value. Under high sedimentation rates, the deposition is increasing along the mountain front and this leads to high  $Smf$  values.

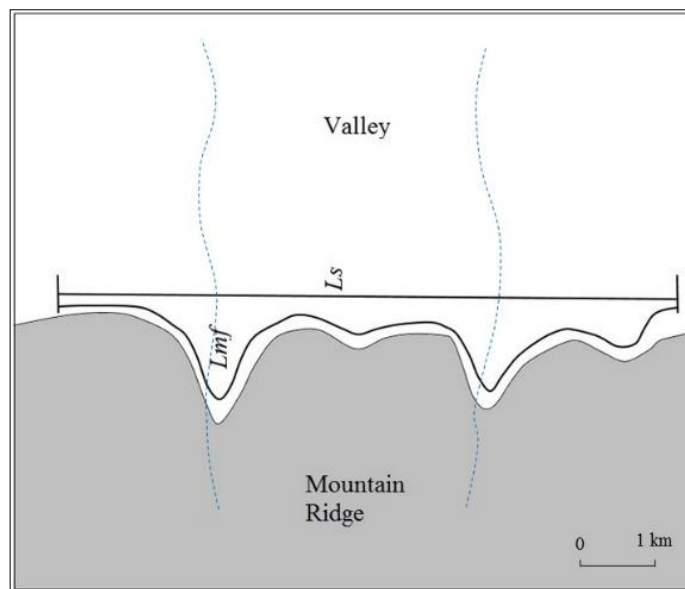


Figure 4.9. Sketch draw showing how mountain front sinuosity ( $Smf$ ) is calculated (modified from Keller & Pinter, 2002).

Within the study area, the Smf index was calculated at three locations. These are respectively along the Manisa Fault, along the northeastern of Gölarmara Ridge, and along the northeast margin of the Çaldağ Ridge (Figure 4.10). The Smf value for the Manisa Fault was calculated as 1.21 and for the Gölarmara the value was obtained as 1.17. The Smf value for the Çaldağ was calculated as 1.50.

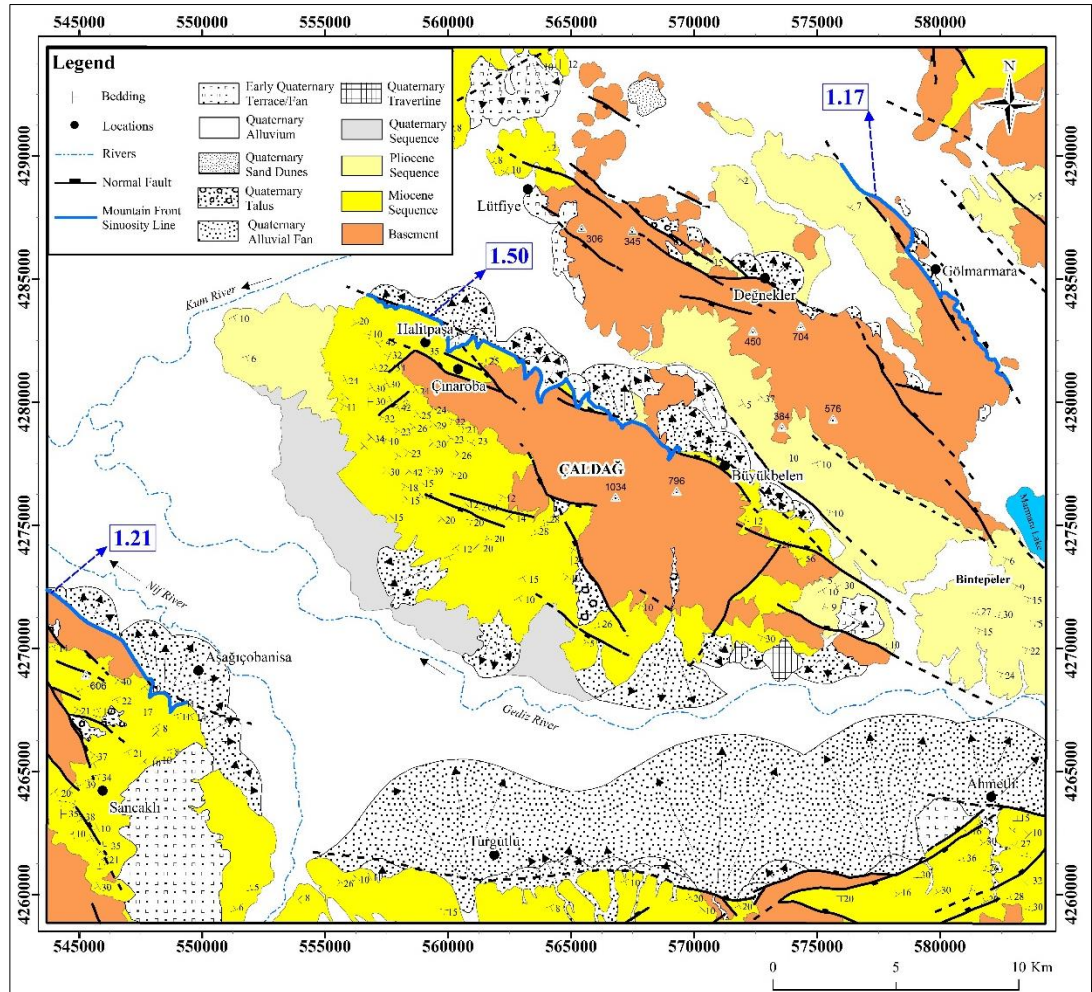


Figure 4.10. The map showing where the Smf index has been calculated with their results. The Smf value of the Manisa Fault is 1.21; the Smf value of the northeast margin of the Çaldağ is 1.50; the Smf value of the northeastern of the Gölarmara Ridge is 1.17.



## CHAPTER 5

### DISCUSSION

The attitude of the bedding planes was conducted on Pliocene and Miocene sequences. While one dominant strike trend was determined for Pliocene sequence, two dominant strike trends were determined for Miocene sequence from the rose diagrams. The main reason for this difference is related to the bedding planes which are controlled by the faults. In the study area, the fault activities occurred at Miocene sequence especially at south of Çaldağ, at Spil Mountain, and around Turgutlu-Ahmetli region. That's why the strike trend difference is observed at Miocene sequence.

The GAG was the subject to the fault lineation studies and these studies were carried out at different locations of the graben. Çiftçi and Bozkurt (2009a) studied the southeastern margin of the GAG around Alaşehir and mentioned that the fault sets show clustering of strike orientations predominantly in WNW-ESE direction but also in NE-SW and NW-SE directions. These orientations are showing parallelism with the three fault clusters determined in the study area. This situation indicates that the faults developed within the graben have same orientation directions mainly. From southeast to the center of the graben, the orientation is dominantly in WNW-ESE direction.

In order to understand the relation between the bedding planes and the faults, they should be evaluated together. Fault trend and bedding trends show parallelism to each other within the study area generally as it can be understood from the dominant strike trend results. The bedding plane trends of the Miocene sequence at the southwestern part of the Çaldağ is parallel to the faults along the northeastern part of the Çaldağ. However, this parallelism is not true for the trends of the Miocene sequences located between Ahmetli and Sancaklı (SE of Manisa). Between these regions, the trend of the sequences is differently related to the general fault trend. The bedding planes

trends of the Pliocene sequences at the southeastern of the Değnekler show almost parallelism to the fault trends observed along the Değnekler and the Gölarmara.

The fault planes determined within the study area were evaluated kinematically.  $\sigma_1$  and  $\sigma_3$  were the main evaluating tool in this study. The stress regime and the fault type depending on the vertical principal stress axis were determined.  $\sigma_1$  was defined as almost vertical on stereoplot views at the locations where the kinematic analyzes were carried out. According to this verticality, the stress regime is extensional, and the fault type is a normal fault. The R-value shows pure extension dominantly in NNE-SSW direction within the study area. The kinematic analyzes were subject of many studies within the GAG. Temiz et al. (1998) evaluated the kinematic analyzes of normal faults in the southeastern part of the GAG. According to their analyzes, there are two Neogene extension directions that are N-S and NNE-SSW. The kinematic analyzes of normal faulting indicated dominantly NNE-SSW extension in Pleistocene deposits (Temiz et al., 1998). Çiftçi and Bozkurt (2009a) indicated approximately N-S extension varying in the range of NNE-SSW and NNW-SSE in the southeastern margin of the GAG. These indicate that the faulting of the GAG is under the control of same fault mechanism because of same extension direction from the southeast of the graben to the west.

The Manisa Fault was studied along the Manisa-Turgutlu highway from northwest to southeast. The fault slip-data were used to evaluate the faults kinematically. Same study was conducted by Bozkurt and Sözbilir (2006) at two locations named as Location 1 (representing Location 01 of the Manisa Fault in this study) and Location 2 (representing Location 03 of the Manisa Fault in this study). The main motion along the fault planes was defined as normal, but the existence of an earlier sinistral strike-slip motion with minor normal component was determined by Bozkurt and Sözbilir (2006). In earlier strike slip motion, there is a compression in E-W direction and an extension in N-S direction. As the main motion along the fault planes, the normal fault was evaluated kinematically in two location by Bozkurt and Sözbilir (2006). They defined the Manisa Fault as a single fault with a short bend along strike at Location 1

and in this context, the kinematic analysis was carried out in three parts as in this study. The results indicate approximately NE-SW extension. In this study, the extension was defined approximately in N-S to NNE-SSW direction. In Location 2 of Bozkurt and Sözbilir (2006), the kinematic analysis indicate approximately ENE-WSW extension direction and in this study the extension was defined in NE-SW direction. As a result, when the kinematic results of the Manisa Fault determined in this study were compared with those of Bozkurt and Sözbilir (2006), it is defined that there is a parallelism with each other. Thus, it is said that along the Manisa Fault there is approximately NNE-SSW extension.

Asymmetry along the ridges was studied in two ways. Firstly, the slope analysis along the mountain ridges have been defined and secondly, the asymmetry ratio of the ridges have been evaluated. In order to understand the slope changes along the ridges, the slope values were combined with each other according to the slope intervals (Table 4.1), and the slope map model was created (Figure 5.1). This map indicates the slope changes at both sides of the ridges. Basically, along the mountain ridges the Quaternary unit development is still continuing and covers wide region. At Quaternary units, the slope values are between  $0^{\circ}$  and  $2^{\circ}$ . This slope change is defined as gentle slope at Quaternary units around the ridges. At Neogene sequences, the slope becomes steeper than the slope at Quaternary units. The slope increases at the points where the basement starts in the profiles. The most important factor affecting the slope change is accepted as the fault activity. The slope increases related to fault activity are seen at *Profile 04, Profile 06, Profile 08, Profile 10, and Profile 12* for the Çaldağ Ridge; at *Profile 16, Profile 18, Profile 20, Profile 22, Profile 24, and Profile 26* for the Değnekler Ridge, at *Profile 30, Profile 32, and Profile 34* for the Gölarmara Ridge. At *Profile 04*, the slope increase is related to the fault evaluated in Çınaroba village. At other profiles defined above for the Çaldağ Ridge, the slope increase is related to the fault having the same mechanism with the fault evaluated in Halitpaşa and Çınaroba villages, and this fault is named as the Büyükbelen Fault. At *Profile 16* for the Değnekler Ridge, the effect of fault evaluated in Lütfiye village causes the slope

increase. Especially at *Profile 22*, the slope increase is related to the fault named as the Değnekler Fault in Değnekler village. The effect of this fault is seen at other profiles defined above for the Değnekler Ridge. At profiles defined above for the Gölarmara Ridge, the slope increase is related to the fault named as the Gölarmara Fault in Gölarmara. Thus, all of this information suggests the fault activity caused the slope increase, and along the northeastern sides of the ridges this effect is seen clearly. By increasing the number of profiles, the accuracy of the slope map model can be increased. The asymmetry ratio was applied as a second way for all ridges according to the width of profiles. The determination of knick-points is the important step of this method. The Quaternary units defined at profiles were determined as knick-point because the Quaternary units are continuously developing within the study area. This means that , the exact width of the profiles is changing continuously. There are no results equal to 1 (Table 4.3). Where the result is less than 1, the imaginary symmetry line is moving towards the northeast.

The Mountain Front Sinuosity index (Smf) values vary at three locations within the study area. If the Smf value is less than 1.4, there is generally an active faulting (Bull and McFadden, 1977). According to this definition, the Smf values of the Manisa Fault and the Gölarmara is less than 1.4 and it is said that there are active faulting at these two locations. Özkaymak and Sözbilir (2012) calculated the Smf value as averagely 1.12-1.14 at same region along the Manisa Fault. Eski (2014) calculated the Smf value as 1.20 along the Gölarmara, and these results also indicate active faulting in the region. The reasons for higher value at Çaldağ depend on two main factors that are erosion resistance and sedimentation rate. Along the Çaldağ where the Smf was calculated the lithology is mainly Miocene sequence which consists of generally sedimentary units. Moreover, along the Çaldağ the alluvial fan deposition is continuing. These two situations affect the Smf value index and increase the results. Because the Smf result is greater than 1.4 along the Çaldağ, it is said that there is less active faulting.

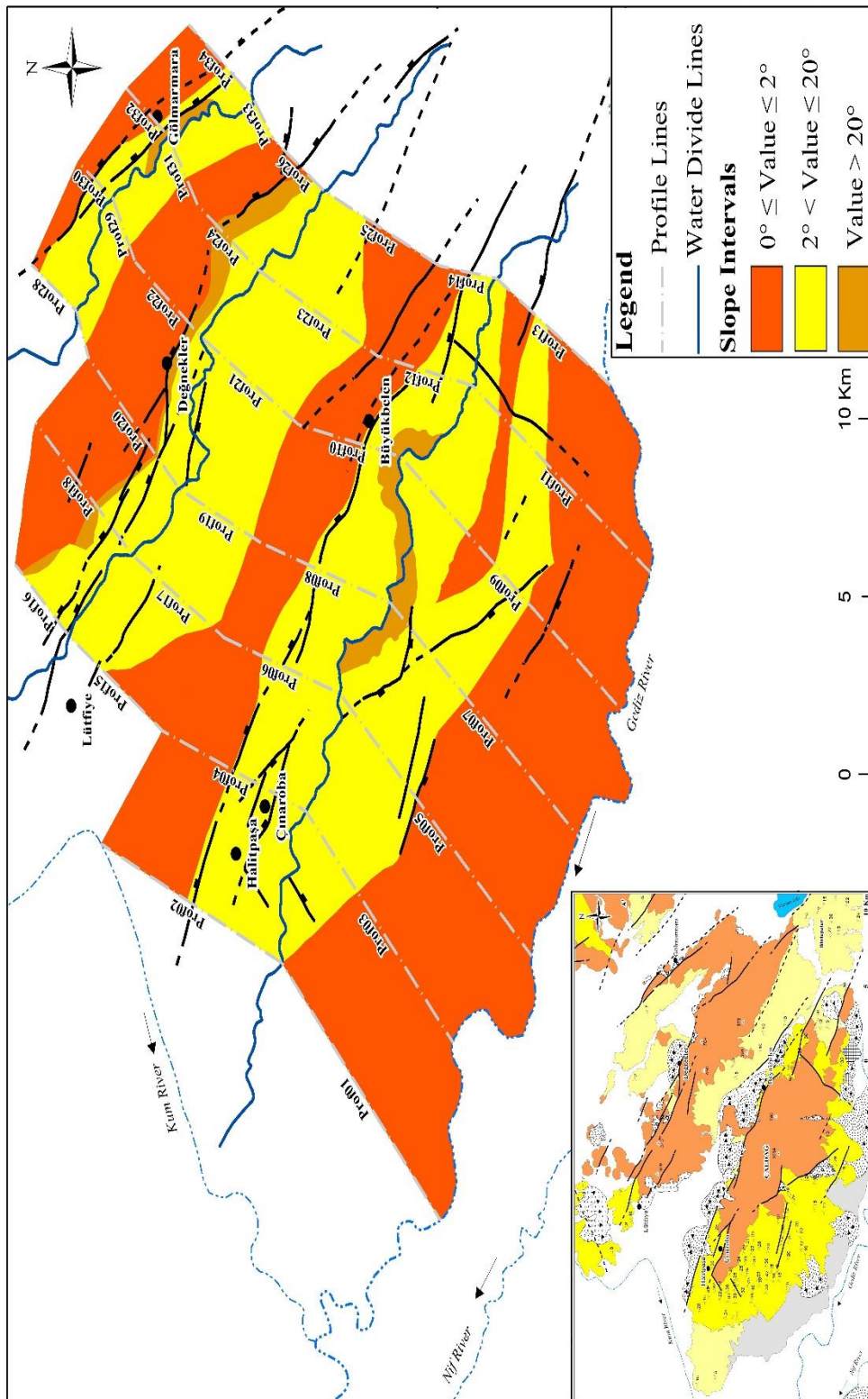


Figure 5.1. The slope map model created for three mountain ridges according to determined slope changes in the profiles.



## CHAPTER 6

### CONCLUSION

#### 6.1. Results of Structural Geology

- The most dominant trend of the Pliocene sequence determined from the rose diagram is between 100°N and 120°N (WNW-ESE).
- The most dominant and second dominant trends of the Miocene sequence determined from the rose diagram are 120°N and 140°N (NW-SE) and 60°N and 80°N (ENE-WSW).
- Three main clusters have been determined for the fault attitude from the length weighted rose diagram. The first cluster is between 120°N-130°N (ESE-WNW), the second cluster is between 140°N-150°N (NNW-SSE) and the third cluster is between 50°N-70°N (ENE-WSW).
- The first cluster is observed along the Büyükbelen Fault located at the Çaldağ, the Değnekler Fault, and the Manisa Fault; the second cluster is observed along the Gölarmara Fault and the faults evaluated at northeast of the Gölarmara; the third cluster is observed at south of Ahmetli, and at southeast of the Çaldağ.
- The study area is showing dominantly NNE-SSW extension.
- The faults evaluated kinematically within the study area are normal faults because  $\sigma_1$  was determined as almost vertical on stereoplot views.
- The faults evaluated in Halitpaşa and Çınaroba show actually the main fault mechanism of the Büyükbelen fault located along the northeastern of the Çaldağ.
- The Çaldağ is under the control of two normal faults, and there is a horst formation.
- The faults evaluated in Lütfiye and Değnekler are normal faults and indicate the main fault mechanism of the Değnekler Ridge.

- The Gölarmara Fault is defined as the normal fault along the Gölarmara Ridge.
- Between Çaldağ and Değnekler Ridges, and between Değnekler and Gölarmara Ridges, there are half-graben formations because of the normal faults.
- The Karahöyük Mountain is under the control of two normal faults, and the Karahöyük Mountain is rising between these two faults. WNW-ESE trending Karahöyük Mountain is a horst structure in the GAG.

## **6.2. Results of Morphometric Analysis**

- The Quaternary units are growing continuously within the study area, and the slope of these units generally is between 0° and 2°.
- Along the Çaldağ, the Değnekler, and the Gölarmara Ridges, the northeastern slopes are under the control of the faults.
- The slope is becoming steeper towards the basement unit.
- The asymmetry ratio results are less or greater than 1, and for three mountain ridges it is said that they are asymmetric. The results that are less than 1 indicate that the symmetry line is shifting towards northeast.
- The main reason for the asymmetry is the fault activity along the northeast side of the mountain ridges.
- The Smf values are 1.21 along the Manisa Fault; the Smf value is 1.50 along the northeast margin of the Çaldağ; the Smf value is 1.17 along the northeast of the Gölarmara.
- Because the Smf values along the Manisa Fault and the Gölarmara Fault are less than 1.4, it is said that there are active faulting.
- Because the Smf value is greater than 1.4 at Çaldağ, the region shows less active faulting.

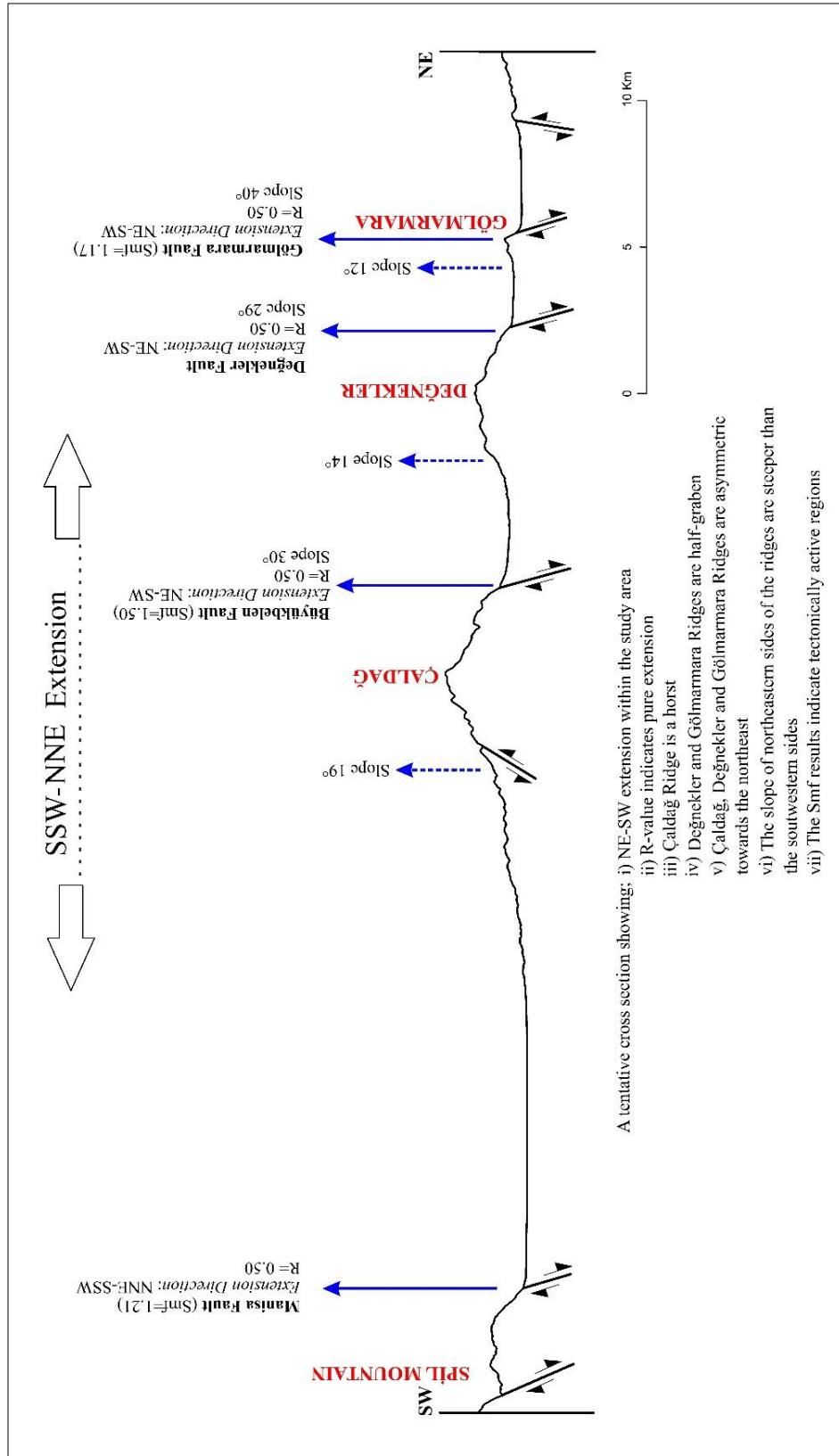


Figure 6.1. A tentative cross section along the study area.

A tentative cross section is showing all obtained results along the study area (Figure 6.1). The Çaldağ Ridge is a horst. Değnekler and Gölarmara Ridges are half graben. According to the Smf results, the region is tectonically active along the Manisa Fault and the Gölarmara fault. The ridges are asymmetric towards northeast.

To sum up, the GAG is constructed by i) faults with the results of NW-SE trending lineaments and NE-SW pure extension from kinematic analysis, ii) active faults by morphometric analysis done on asymmetry along the ridges and the mountain front sinuosity, iii) active faults with travertine accumulation (eg. in Canbazlı village located at the southeastern of the Çaldağ, in Harmandalı located at the northeastern of the Gölarmara), and iv) being in a seismically active region.

## REFERENCES

- Angelier, J., & Mechler P. (1977). Sur une methode graphique de recherche des contraintes principales egalement utilisable en tectonique et en seismologie: la methode des dibdres droits. *Bull. Soc. Geol. Fr.*, 7(19), 1309-1318.
- Azor, A., Keller, E. A., & Yeats, R. S. (2002). Geomorphic indicators of active fold growth: South Mountain-Oak Ridge anticline, Ventura Basin, southern California. *Geological Society of American Bulletin*, 114(6), 745-753.
- Bozkurt, E. (2001). Neotectonics of Turkey – a synthesis. *Geodinamica Acta*, 14, 3-30.
- Bozkurt, E., & Rojay, B. (2005). Episodic, tow-stage Neogene extension and short-term intervening compression in western Anatolia: field evidence from the Kiraz Basin and Bozdağ Horst. *Geodinamica Acta*, 18 (3-4), 295-312.
- Bozkurt, E. & Sözbilir, H. (2006). Evolution of the Large-scale active Manisa Fault, Southwest Turkey: Implications on fault development and regional tectonics. *Geodinamica Acta*, 19 (6), 427-453.
- Bull, W.B. (1977). Tectonic geomorphology of the Mojave Desert. U.S. Geological Survey Contract Report 14-08-001-G-394. Office of Earthquakes, Volcanoes, and Engineering: Menlo Park, CA.
- Bull, W. B., & McFadden, L.D. (1977). Tectonic geomorphology north and south of the Garlock fault, California. In: D. O. Doethering (Ed.), *Geomorphology in arid regions. Proceeding at the Eighth Annual Geomorphology Symposium*, 115-138. State University of New York, Binghamton, NY.
- Burg, J. P. (2017). Paleo- “STRESS” Analysis from fault data. Retrieved from <http://www.files.ethz.ch/structuralgeology/JPB/files/English/>
- Çiftçi, N. B. & Bozkurt, E. (2007). Anomalous stress field and active breaching at relay ramps: A field example from Gediz Graben, SW Turkey. *Geological Magazine*, 144 (4), 687-699, doi: 10.1017/S0016756807003500.
- Çiftçi, N. B. & Bozkurt, E. (2009a). Pattern of normal faulting in the Gediz Graben, SW Turkey. *Tectonophysics*, 473, 234-260.
- Çiftçi, N. B. & Bozkurt, E. (2009b). Evolution of the Miocene sedimentary fill of the Gediz Graben, SW Turkey. *Sedimentary Geology*, 216, 49-79.
- Delvaux, D. (1993). The TENSOR program for paleostress reconstruction: examples from the east African and the Baikal rift zones. EUGVII Strasbourg, France, 4-8 April 1993. *Terra Nova*, 5, 216.

- Delvaux, D., Moeys, R., Stapel, G., Petit, C., Levi, K., Miroshnichenko A., Ruzhich, V., & San'kov, V. (1997). Paleostress reconstructions and geodynamics of the Baikal region, Central Asia, Part 2. Cenozoic rifting. *Tectonophysics*, 282, 1-38.
- Dewey, J.F. and Şengör, A.M.C., (1979). Aegean and surrounding region: Complex multiplate and continuum tectonics in a convergent zone. *Geological Society of America Bulletin*, 90, 84-92.
- Emre, T. (1996). Gediz Grabeni'nin tektonik oluşumu. *Türkiye Jeoloji Bülteni*, 29 (2), 1-18.
- Erdoğan, B., 1990; İzmir-Ankara Zonunun İzmir ile Seferihisar arasındaki bölgede stratigrafik özellikleri ve tektonik evrimi. TPJD Bülteni, 2/1, 1-20.
- Eski, S. (2014). Gölarmara havzasının (Gediz Grabeni kuzey kolu) aktif tektoniği, Manisa. Dokuz Eylül Üniversitesi Fen Bilimleri Enstitüsü. Doi: 10.13140/RG.2.219187.02080.
- Helvacı, C., Gündoğan, İ., Oyman, T., Sözbilir, H. & Parlak, O. (2013). Çaldağ (Turgutlu-Manisa) lateritik Ni-Co yatağının jeolojisi, mineralojisi ve jeokimyasal özellikleri. *Yerbilimleri*, 34(2), 101-132.
- Kahle, H., Straub, C., Reilinger, R., McClusky, S., King, R., Hurst, K., Veis, G., Kastens, K., & Cross, P. (1998). The strain rate field in the eastern Mediterranean region, estimated by repeated GPS measurements. *Tectonophysics*, 294, 237-252.
- Keller, E. A., & Pinter, N. (2002). *Active Tectonics Earthquakes, Uplift, and Landscape*. NJ: Prentice Hall, Upper Saddle River, (p. 362).
- Kent, E., Boulton, S. J., Stewart, I. S., Whittaker, A. C., & Alçiçek, M. C. (2016). Geomorphic and geological constraints on the active normal faulting of the Gediz (Alaşehir) Graben, Western Turkey. *Journal of the Geological Society*, 173, 666-678, doi: 10.1144/jgs2015-121.
- Kent, E., Boulton, S. J., Stewart, I. S., Whittaker, A. C., & Alçiçek, M. C. (2017). Normal fault growth and linkage in the Gediz (Alaşehir) Graben, Western Turkey, revealed by transient river long-profiles and slope-break knickpoints. *Earth Surface Processes and Landforms*, 42, 836-852, doi: 10.1002/esp.4049.
- Koçyiğit, A., Yusufoglu, H., & Bozkurt, E. (1999). Evidence from the Gediz graben for episodic two-stage extension in western Turkey. *Journal of the Geological Society*, 156, 605-616.
- Le Pichon, X., & Angelier, J. (1979). The Hellenic Arc and trench system: a key to the Neotectonic evolution of the eastern Mediterranean area. *Tectonophysics*, 60, 1-42.

- McClusky, S., Balassanian, S., Barka, A., Demir, C., Ergintav, S., Georgiev, I., Gürkan, O., Hamburger, M., Hurst, K., Kahle, H., Kastens, K., Kekelidze, G., King, R., Kotzev, V., Lenk, O., Mahmoud, S., Mishin, A., Nadariya, M., Ouzonunis, A., Paradissis, D., Peter, Y., Prilepin, M., Reilinger, R., Sanli, I., Seeger, H., Tealeb, A., Toksöz, M.N., & Veis, G. (2000). Global Positioning System constraints on plate kinematics and dynamics in the eastern Mediterranean and Caucasus. *Journal of Geophysical Research*, *105*, 5695-5719.
- McKenzie, D. (1978). Active tectonics of the Alpine-Himalayan belt: the Aegean Sea and surrounding regions. *Geophysical Journal of the Royal Astronomical Society*, *55*, 217-254.
- Meulenkamp, J. E., Wortel, M. J. R., Van Wamel, W. A., Spakman, W. & Strating, E. H. (1988). On the Hellenic subduction zone and the geodynamic evolution of Crete since the late Middle Miocene. *Tectonophysics*, *146*, 203-215.
- Özkaymak, Ç. (2015). Tectonic analysis of the Honaz Fault (western Anatolia) using geomorphic indices and the regional implications. *Geodinamica Acta*, *27*, 109-128.
- Özkaymak, Ç., & Sözbilir, H. (2008). Stratigraphic and structural evidence for fault reactivation: The active Manisa fault zone, western Anatolia. *Turkish Journal of Earth Sciences*, *17*, 615-635.
- Özkaymak, Ç., & Sözbilir, H. (2012). Tectonic geomorphology of the Spildağı High Ranges, western Anatolia. *Geomorphology*, *173-174*, 128-140.
- Özkaymak, Ç., Sözbilir, H., & Uzel, B. (2013). Neogene-Quaternary evolution of the Manisa Basin: Evidence for variation in the stress pattern of the İzmir-Balıkesir Transfer Zone, western Anatolia. *Journal of Geodynamics*, *65*, 117-135.
- Özkaymak, Ç., Sözbilir, H., Uzel, B., & Akyüz, H. S. (2011). Geological and Palaeoseismological Evidence for Late Pleistocene-Holocene Activity on the Manisa Fault Zone, Western Anatolia. *Turkish Journal of Earth Sciences*, *20*, 449-474.
- Reilinger, R. E., McClusky, S. C., Oral, M. B., King, R. W., Toksoz, M. N., Barka, A. A., Kinik, I., Lenk, O., & Şanlı, I. (1997). Global Positioning System measurements of present-day crustal movements in the Arabia-Africa-Eurasia plate collision zone. *Journal of Geophysical Research*, *102*, 9983-9999.

- Reilinger, R., McClusky, S., Vernant, P., Lawrence, S., Ergintav, S., Çakmak, R., Özener, H., Kadirov, F., Guliev, İ., Stepanyan, R., Nadariya, M., Hahubia, G., Mahmoud, S., Sakr, K., ArRajehi, A., Paradissis, D., Al-Aydrus, A., Prilepin, M., Guseva, T., Evren, E., Dmitrotsa, A., Filikov, S.V., Gomez, F., Al-Ghazzi, R., & Karam, G. (2006). GPS constraints on continental deformation in the Africa-Arabia-Eurasia continental collision zone and implications for the dynamics of plate interactions. *Journal of Geophysical Research*, *111*, doi: 10.1029/2005JB004051.
- Rojay, B. & Toprak, V. (2001). Neogene Evolution of the Gediz Graben, Western Anatolia, Turkey. Riotur Internal Report.
- Sarıkaya, M. A. (2004). Gediz ayrılma zonu: Fay kayacı stratigrafisi ve tektonik önemi. *Yerbilimleri*, *30*, 63-79.
- Seyitoğlu, G., & Scott, B. C. (1991). Late Cenozoic crustal extension and basin formation in west Turkey. *Geological Magazine*, *128*, 155-166.
- Seyitoğlu, G., & Scott, B. C. (1992). The age of the Büyük Menderes graben (west Turkey) and its tectonic implications. *Geological Magazine*, *129*, 239-242.
- Seyitoğlu, G., & Scott, B. C. (1996a). The cause of N-S extensional tectonics in western Turkey: Tectonic escape vs. back-arc spreading vs. orogenic collapse. *Journal of Geodynamics*, *22*, 145-153.
- Seyitoğlu, G., & Scott, B. C. (1996b). Age of the Alaşehir graben (west Turkey) and its tectonic implications. *Geological Journal*, *13*, 1-11.
- Seyitoğlu, G., Tekeli, O., Çemen, İ., Şen, Ş., & Işık, V. (2002). The role of the flexural rotation/rolling hinge model in the tectonic evolution of the Alaşehir graben, western Turkey. *Geological Magazine*, *139* (1), 15-26.
- Sözbilir, H. (2001). Extensional tectonics and the geometry of related macroscopic structures: field evidence from the Gediz Detachment, Western Turkey. *Turkish Journal of Earth Sciences*, *10*, 51-67.
- Süzen, M. L., Toprak, V., & Rojay, B. (2006). High-altitude Plio-Quaternary fluvial deposits and their implication on the tilt of a horst, western Anatolia, Turkey. *Geomorphology*, *74*, 80-99.
- Şengör, A. M. C., Görür, N., & Şaroğlu, F. (1985). Strike-slip faulting and related basin formation in zones of tectonic escape: Turkey as a case study. In: K. Biddle, N. Christie-Blick (eds), *Strike-slip Deformation, Basin Formation and Sedimentation. Society of Economic Paleontologists and Mineralogists, Special Publications*, *37*, 227-264.
- Şengör, A. M. C., & Yılmaz, Y. (1981). Tethyan Evolution of Turkey: A Plate Tectonic Approach. *Tectonophysics*, *75*, 181-241.

- Şengör, A. M. C. (1985). Cross-faults and differential stretching of hanging walls in regions of low-angle normal faulting: examples from western Turkey. *Geological Society, London, Special Publications*, 28, 575-589.
- Temiz, H., Gürsoy, H., & Tatar, O. (1998). Kinematics of Late Pliocene-Quaternary normal faulting in the southern end of the Gediz Graben, Western Anatolia, Turkey. *International Geology Review*, 40, 638-646.
- Tepe, Ç., & Sözbilir, H. (2017). Tectonic geomorphology of the Kemalpaşa Basin and surrounding horsts, southwestern part of the Gediz Graben, Western Anatolia. *Geodinamica Acta*, 29, 70-90.
- Topal, S. (2019a). Karacasu Fayı'nın (GB Türkiye) göreceli tektonik aktivitesinin jeomorfik indislerle incelenmesi. *GÜFBED*, 9(1), 37-48.
- Topal, S. (2019b). Evaluation of relative tectonic activity along the Priene-Sazlı Fault (Söke Basin, southwest Anatolia): Insights from geomorphic indices and drainage analysis. *Journal of Mountain Science*, 16(4), 909-923.
- Topal, S., & Özkul M. (2018). Determination of relative tectonic activity of the Honaz fault (SW Turkey) using geomorphic indices. *Pamukkale Üniversitesi Mühendislik Bilimleri Dergisi*, 24(6), 1200-1208.